UNIVERSITY OF TURIN
DEPARTMENT OF MEDICAL SCIENCES

PhD in Biomedical Sciences and Oncology

Curriculum Advanced Techniques for the Localization of Human Tumors

(2015-2019) - XXXI cycle

PhD Dissertation

Subcellular characterization of NAD^+ biosynthesis in metastatic melanoma by using organelle-specific biosensors

Candidate: Dr. Federica GAUDINO

Supervisor: Prof. Silvia DEAGLIO

PhD program Coordinator: Prof. Emilio HIRSCH

Academic Year 2019-2020

Abstract

NAD^+ plays central roles in a wide array of normal and pathological conditions. Inhibition of NAD^+ biosynthesis can be exploited therapeutically in cancer, including melanoma. To obtain quantitation of NAD^+ levels in live cells and to address the issue of the compartmentalization of NAD^+ biosynthesis, we exploited a recently described, genetically-encoded NAD^+ biosensor (LigA-cpVENUS), which was targeted to the cytosol, mitochondria and nuclei of BRAF-V600E A375 melanoma cells, a model of metastatic melanoma (MM). FK866, a specific inhibitor of nicotinamide phosphoribosyltransferase (NAMPT), the main NAD^+-producing enzyme in MM cells, was used to monitor NAD^+ depletion kinetics at the subcellular level in biosensor-transduced A375 cells. In addition, we treated FK866-blocked A375 cells with NAD^+ precursors, including nicotinamide, nicotinic acid, nicotinamide riboside and quinolinic acid, highlighting an organelle-specific capacity of each substrate to rescue from NAMPT block. Expression of NAD^+ biosynthetic enzymes was then biochemically studied in isolated organelles, revealing presence of NAMPT in all three cellular compartments, while NAPRT was predominantly cytosolic and mitochondrial, and NRK mitochondrial and nuclear. In keeping with biosensor data, QPRT was expressed at extremely low levels. Throughout this work, we validated the use of genetically encoded NAD^+ biosensors to characterize subcellular distribution of NAD^+ production routes in MM. The chance of real time monitoring of NAD^+ fluctuations after chemical perturbations, together with a deeper comprehension of the cofactor biosynthesis compartmentalization, strengthens the foundation for a targeted strategy of NAD^+ pool manipulation in cancer and metabolic diseases.

Abbreviations Used

3PG = glyceraldehyde-3-phosphate;3-phosphoglycerate

6PGD= phosphogluconate dehydrogenase

αKG = alpha-ketoglutarate

A375/S = A375 sensitive to BRAF inhibitors

A375/BiR = A375 resistant to BRAF inhibitors

ADP= adenosine diphosphate

ADPR = ADP ribose

cADPR = cyclic ADP ribose

CIT = citrate

cisACT = cis-aconitate

CoQ = Coenzyme Q

AlaM = alamethicin

ARTs = adenosine diphosphate (ADP)-ribose transferases

ATP = adenosine triphosphate

BRAFi = BRAF inhibitor

cpVENUS = circularly permutated Venus protein

ETC = electron transport chain

F1,6BP = fructose-1,6-bisphosphate

F6P = Fructose-6-phosphate

FUM = fumarate

GAPDH = glyceraldehyde phosphate dehydrogenase

G6DP = glucose-6-phosphate dehydrogenase

GR = glutathione reductase

GSH = glutathione

GSSG = oxidized glutathione

HPLC = high performance liquid chromatography

IDH = isocitrate dehydrogenase

isoCIT = isocitrate

LDH = lactate dehydrogenase

MAL = malonate,

MDH = malate dehydrogenase

MM = metastatic melanoma

NA = nicotinic acid

NAD^+ =nicotinamide adenine dinucleotide

NAAD = nicotinate adenine dinucleotide

NAADP = nicotinic acid adenine dinucleotide phosphate

NADH = reduced nicotinamide adenine dinucleotide

NADP = nicotinamide adenine dinucleotide phosphate

NADPH = reduced nicotinamide adenine dinucleotide phosphate

NAM = nicotinamide

NaMN = nicotinic acid mononucleotide

NAMPT = nicotinamide phosphoribosyltransferase

NAMPTis = nicotinamide phosphoribosyltransferase inhibitors

NAPRT = nicotinate phosphoribosyltransferase

NBEs = NAD^+ biosynthetic enzymes

Ndt1p = mitochondrial NAD^+ carrier protein

NMN = nicotinamide mononucleotide

NMNAT = nicotinamide mononucleotide adenylyltransferase

NR = nicotinamide riboside

NRK = nicotinamide riboside kinase

OA = phosphoenolpyruvate;oxaloacetate,

OGD = oxoglutarate dehydrogenase

PARPs = poly (ADP-ribose) polymerases

PDC = pyruvate dehydrogenase complex

PRPP = phosphoribosylpyrophosphate

QA = quinolinic acid

QPRT = quinolinate phosphoribosyltransferase

SIRTs = sirtuins

SUCCoA = succinylCoA,

SUC = succinate

TCA = tricarboxylic acid cycle

TR = thioredoxin reductase

Trx = thireoxidin

Table of Contents

Introduction

1.1 NAD^+ metabolism

1.1.1 The multifaceted role of NAD^+

Nicotinamide adenine dinucleotide (NAD^+) is a vital, ubiquitous and multifunctional cofactor regulating a wide range of biological processes (19,47). Discovered more than a century ago as cofactor in fermentation, knowledge about chemistry and function of NAD^+ was improved after the seminal discoveries of Otto Warburg in 1930s (11). The relevance of findings concerning the centrality of NAD^+ reactions in cell physiology, strongly encouraged studies on NAD^+ metabolism in the last decades, leading to the validated evidence of the multifaceted role of NAD^+ as energy cofactor and signalling molecule (47) (Figure 1).

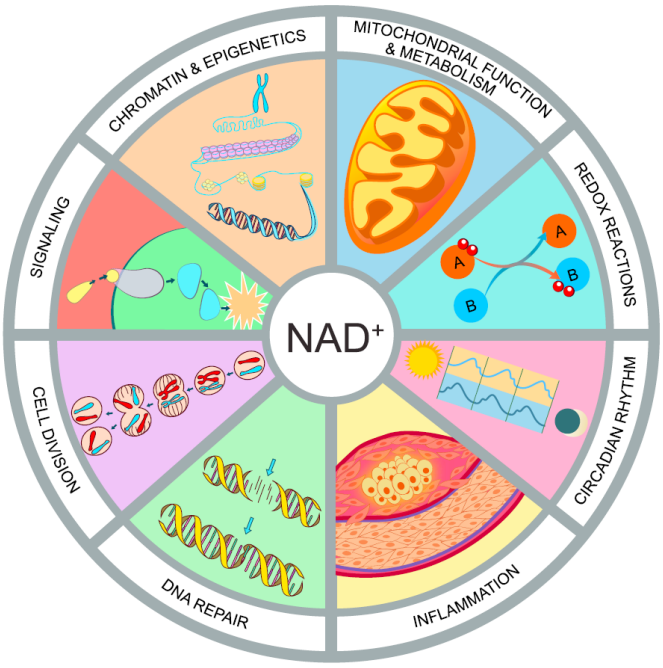

Figure 1. Hallmarks of NAD^+ Homeostasis. NAD^+ is both a redox co-factor and a key signalling molecule. It controls mitochondrial function and metabolism, redox reactions, circadian rhythm, immune response and inflammation, DNA repair, cell division, cell survival, chromatin stabilization and epigenetics.

From Rajman L. et al., Cell Metabolism Review 2018 (79).

1.1.2 The energetic role of NAD^+

As energetic co-enzyme, NAD^+ is essential as electron acceptor donor in various metabolic pathways including cytosolic glycolysis, serine biosynthesis, mitochondrial tricarboxylic acid cycle (TCA) and oxidative phosphorylation redox reactions (103). In addition, the equilibrium existing between its oxidized (NAD^+) and reduced forms (NADH) mediates cellular antioxidation mechanisms, as well as cell redox state homeostasis, energy metabolism and mitochondrial functions (104).

Cofactor of almost 300 dehydrogenase, NAD^+ is primary used during glycolysis in the sixth step of the process by glyceraldehyde phosphate dehydrogenase (GAPDH) which requires two molecules of NAD^+ per molecule of glucose to oxidize glyceraldehyde-3-phosphate to 1,3-biphosphoglycerate (3). Secondly, NAD^+ lactate dehydrogenase (LDH) catalyzes the interconversion of pyruvate and lactate with concomitant interconversion of NADH and NAD^+. The final glycolytic product pyruvate, can be converted to lactate in condition of low oxygen tension or metabolized to produce acetylCoA thus entering the TCA cycle for maximal energy production (2). The pyruvate dehydrogenase complex (PDC) mediates acetylCoA production, a reaction accompanied by NAD^+ reduction to NADH. During TCA cycle NAD^+ is reduced to NADH moieties in several key steps by isocitrate dehydrogenase (IDH), oxoglutarate dehydrogenase (OGD) and malate dehydrogenase (MDH). Finally, NADH produced in all these reactions, working as electron equivalent redistributors, is used by electron transport chain (ETC) to generate ATP (105) (Figure2).

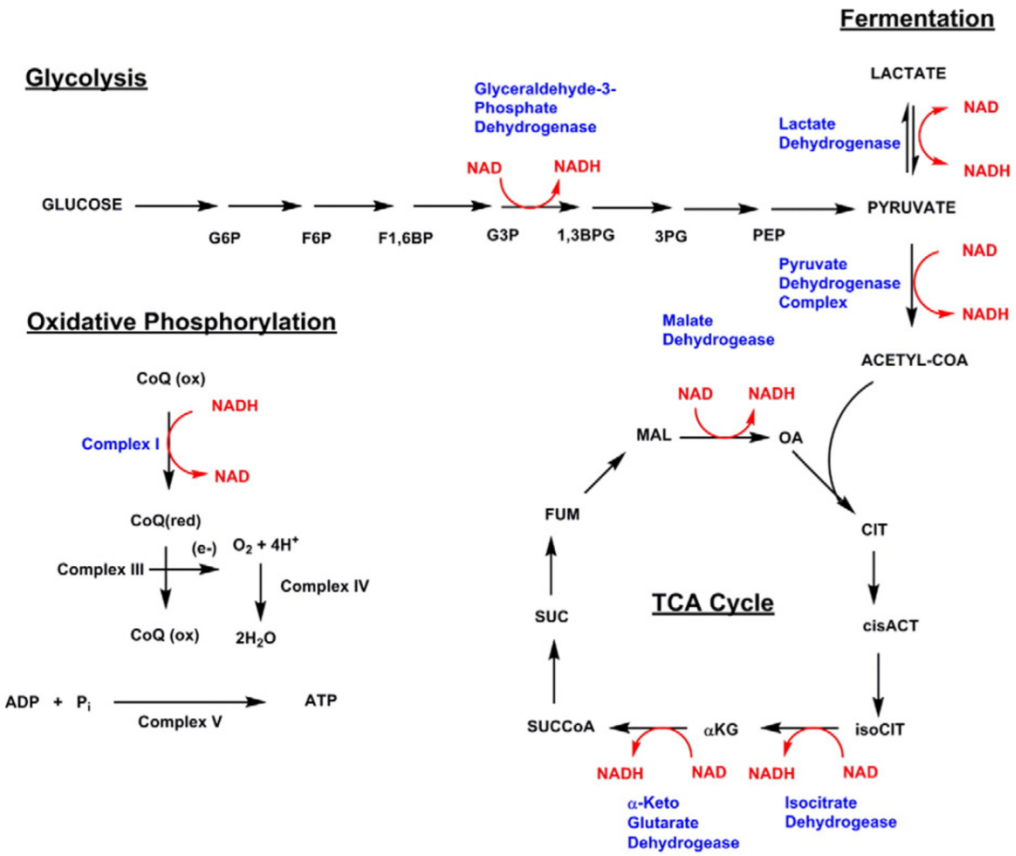

Figure 2. Cellular energy metabolism involving NAD^+/NADH interconversion. *From Yang y, Biochim Biophys Acta (2016) (105).*

The ratio between NAD^+/NADH and their relative phosphorylated form ($NADP^+$/NADPH), are also critical for enzymatic defence systems against oxidative stress (115).

NAD(H) and NADP(H) regulate cellular redox homeostasis through the main cellular scavenging systems which are the glutathione (GSH/GSSG) and the thioredoxin-mediated (Trx-SH/Trx-SS) mechanisms. During these processes, H2O2 is scavenged in reactions carried out by gluthatione and thioredoxin reductases (GS and TR, respectively). Specifically, NADPH donates two electrons to reduce GSSG to GSH by GR; the recycled GSH can then be used to reduce H2O2 to water. On the other hand TRs transfer electrons from NADPH to reduce oxidized thioredoxin (Trx-S2) to its reduced form Trx-(SH)2, which also acts as a donator of reducing equivalents in the enzymatic

removal of H2O2. For these systems a specific subcellular distribution was demonstrated indicating that cytosol is the source of almost 70% of cellular glutathione (40,68,100).

In this context NADPH is the indispensable reducing agent for ROS elimination and redox homeostasis, and also its production is finely compartmentalized between cytosol and mitochondria (100). In the cytosol, NADPH is primarily produced by glucose-6-phosphate dehydrogenase (G6PD) and -phosphogluconate dehydrogenase (6PGD) in the pentose phosphate pathway, while in mitochondria the main source of NADPH is IDH2 (Figure 3). Reports on G6PD-deficient mice and gain-of-function studies deeply showed the protective role of GSPD on cellular function by promoting ROS detoxification thus increasing cell viability. Activity of the enzyme is also post-translationally modulated by the cytosolic sirtuin SIRT2, offering various targetable point for a pharmacological modulation of the system (115).

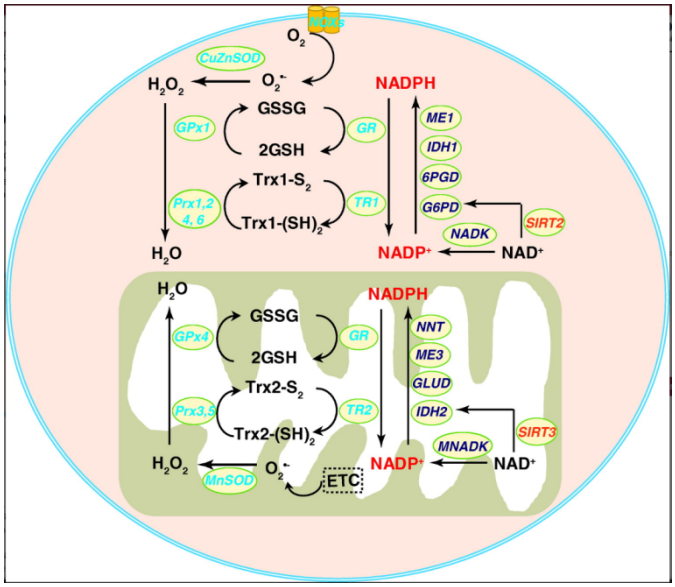

Figure 3. NADPH and NAD^+ function as cofactors in antioxidant defense systems. *From Xiao W. et al., Antiox and Redox (2018) (100).*

1.1.3 NAD^+: a pleiotropic signaling molecule

Independently of its redox properties, NAD^+ is also the substrate of enzymes with fundamental roles in gene expression and cell signaling. In these reactions, NAD^+ is cleaved at the glycosidic bond between nicotinamide and ADP-ribose and, contributing as a donator of ADP-ribose, through its consumption, the energetic cofactor acquires the characteristic of an intracellular or extracellular signaling molecule.

The large family of NAD^+ consuming enzymes includes: mono adenosine diphosphate (ADP)-ribose transferases (ARTs) and poly ADP-ribose polymerases (PARPs) which transfer the ADP ribose moiety to acceptor proteins such as histones, and other proteins at sites of DNA damage, resulting in their modification and function regulation; sirtuins (SIRT1-7) which catalyze the NAD^+-dependent removal of acetyl or acyl groups from lysines of metabolic enzymes and transcription factors, thus controlling their activity; cyclic ADP-ribose hydrolases and NAD^+ glycohydrolase (CD38/CD157 and CD73) that generate different NAD^+ metabolites, like ADP ribose (ADPR), cyclic ADP ribose (cADPR) and nicotinic acid adenine dinucleotide phosphate (NAADP), all molecules with calcium mobilizing properties (44,98) (Figure 4-5).

Through their functional activities of post-translational modifications (ADP-ribosylation and deacetylation reactions), or by calcium (Ca^{2+}) signaling activation, these enzymes regulate gene transcription, cell differentiation, cell cycle progression, circadian rhythm, DNA repair, chromatin stability, cell adaptation to stress signals, immune response (22). The importance of these NAD^+-consuming pathways is demonstrated by the large numbers of therapies, developed over the years, which target these enzymes (Table 1). As an example, PARP inhibitors are in clinical trials as anti-cancer agents, because they can sensitize tumor cells to apoptotic killing by

genotoxic agents, while sirtuins activity is strictly associated with different pathologies occurring with NAD^+ levels decline during aging or neurodegenerative processes (50). For these reasons, NAD^+ boosting molecules or inhibitors of the NADases received remarkable attention as antiaging agents or co-adjuvants for maintaining NAD^+ homeostasis (79). However, as will be described in this dissertation, NAD^+ metabolism is also an attractive therapeutic target in cancer treatment due to the increased levels of the cofactor during tumorigenesis (5,88).

It is certainly possible to affirm that PARPs and sirtuins represent connecting elements between the metabolic state of a cell and its signaling and transcriptional activities. However, to be "metabolic sensors", NAD^+ consuming enzymes have to respond to physiological changes of NAD^+ levels, but the full comprehension of this phenomenon is rendered complex by two incompletely understood aspects of NAD^+ metabolism which are the NAD^+ pool sub-cellular compartmentalization and NAD^+ transport across the cell and organelle membrane (47).

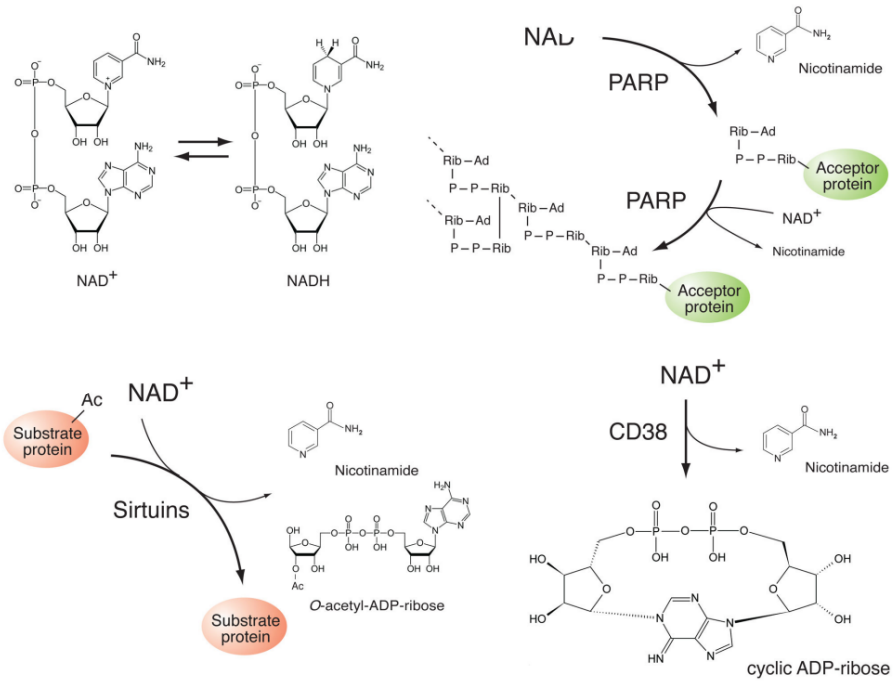

Figure 4. Various uses of NAD^+ for canonical redox and NAD^+-consuming enzymatic reactions. *From Imai S. et al., Trends Cell Biol (2014) (50).*

1.1.4 NAD^+ biosynthesis

The maintenance of cellular NAD^+ level above a critical threshold, is pursued through the re-oxidation from NADH or through the active synthesis of the pyridine nucleotide (Figure 5). Open issues concern the biology of this system, including the subcellular localization of specific biosynthetic pathways. Several efforts were made to elucidate where NAD^+ biosynthesis occurs and whether there are exchanges between compartments (27,28,54,55,69,79).

In details, NAD^+ is synthesized through one *de novo* bio-synthetic pathway, starting from tryptophan/quinolinic acid (QA) and controlled by the rate limiting enzyme quinolinate phosphoribosyltransferase (QPRT) (9,47). This biosynthetic pathway is an 8-steps biosynthesis comprising the so-called kynurenine pathway. The formation of QA occurs in one of the first reactions of this route which is active in mammals, especially in liver and kidney but also in brain and endocrine tissue (109).

To maintain physiological concentration of the vital pyridine cofactor, in parallel, we have three salvage pathways involving i) nicotinamide (NAM), ii) the Preiss-Handler pathway that uses dietary nicotinic acid (NA), iii) and a third process which also uses a food-derived molecule named nicotinamide riboside (NR) (22,62). Each pathway is controlled by a rate-limiting enzyme, specifically nicotinamide phosphoribosyl transferase (NAMPT), nicotinate phosphoribosyltransferase (NAPRT) and nicotinamide riboside kinase (NRK) (Figure 5). NAMPT catalyzes the reaction between NAM and 5-phosphoribosyl-1-pyrophosphate (PRPP) to form nicotinamide mononucleotide (NMN). NMN is then converted to NAD^+ by nicotinamide nucleotide adenyltransferase (NMNAT1-3), using ATP as the donor of adenylyl moiety (62). In parallel, the enzymatic activity of the other players of NAD^+ salvaging consists in the

phosphorylation of NR to NMN performed by NRK, whereas NAPRT phosphoribosylates NA to nicotinate mononucleotide (NAMN) (47). Again the final steps of these reactions are carried out by NMNATs which convert NMN to NAD^+, and NAMN to nicotinate adenine dinucleotide (NAAD). NAAD is finally amidated to NAD^+ by the enzyme NAD^+ synthetase (3) (Figure 5).

Among these pathways, the reaction controlled by NAMPT is the most relevant in mammalian cells (5,81) for NAD^+ homeostasis, as the NAMPT substrate, NAM, is released by the main NAD^+ consuming enzymes, such as sirtuins and PARPs, connecting NAD^+ synthesis and degradation in a functional loop in which NAD^+ is consumed and regenerated (90). NAMPT is widely considered the master regulator of NAD^+ biosynthesis in mammal cells (74), as confirmed by two crucial evidences: the protein expression in all mammal tissues (84) and the embryonically lethality of NAMPT gene deletion in mice (83). Intriguingly, NAMPT was also found in plasma and in the supernatants of different type of cells (tumor cells but also differentiated adipocytes, primary hepatocytes, cardiomyocyte, leucocytes, neutrophils, monocytes and macrophages) where, independently of its catalytic activity, exerts cytokine-like properties (6,47,83,97). While the mechanism behind secretion of extracellular NAMPT (eNAMPT) remain unknown, it is now clear that, released after pro-inflammatory stimuli, eNAMPT levels are increased in pathological conditions such as inflammation and tumors (6,47,83,97). In the extracellular space, NAMPT works as a cytokine able to regulate the differentiation programs and the metabolic adaptation of immune cells, finally driving the cancer-supportive shaping of tumor microenvironment (3,4).

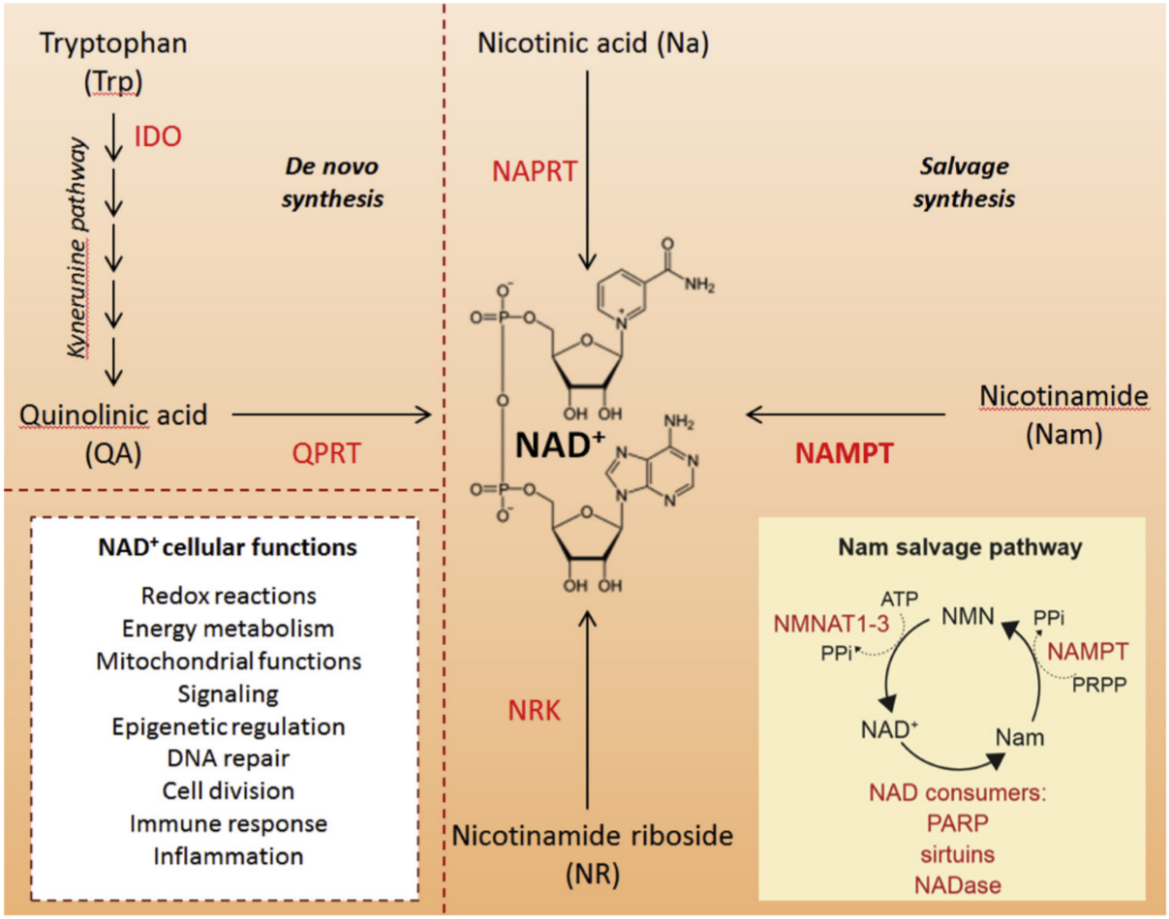

Figure 5. NAD⁺ synthesis, function and consumption. *From Audrito et al 2019 Review* (3).

1.1.5 NAD⁺ pool compartmentalization

The estimated amount of total intracellular NAD⁺ content varies between 200-700 µM (17,19,47,85). Considered one of the most abundant metabolite of human body, NAD⁺ levels constantly fluctuate following cycles of synthesis, consumption, and recycling and change upon specific stimuli (79). Recent studies on NAD⁺ metabolism evidenced that NAD⁺ concentration, oxidative state (NAD⁺/NADH ratio) and protein-associated amount of NAD⁺ differ not only in a tissue-dependent way, but also at sub cellular levels, revealing a specific distributions of NAD⁺ and its precursors in the cytosol, in nuclei and

mitochondria (17,27,55,69). Cytosol and nuclei usually contain similar amount of NAD^+ (100-200 μM) while in mitochondria, NAD^+ levels can reach more than the double (17,19,47,85). Undoubtedly this organelle-compartmentalization is the effect of I) a transport systems for NAD^+ and its precursors in the organelles membrane, ii) an organized distribution of both consuming and NAD^+ biosynthetic pathways, and of iii) the translocation of these enzymes itself which can be temporarily redistributed in a different compartment in order to activate specific pathways responding to cellular demands (55,105).

It is generally accepted that the location and physiological function of a protein are strictly related. Figure 6 shows a recently published representation of current knowledge regarding the sub-cellular compartmentalization of NAD^+ metabolism (55). Looking at the compartmentalization of NAD^+ consuming enzymes, there are 17 members of the PARP family, and they are predominantly located in the nucleus (PARP 1-5, 9 and 14) where there is the majority of PARPs substrates (protein involved in DNA synthesis and repair). Other PARPs are also in cytoplasm (PARP-5,10,12,13,15), in the cell membrane and endoplasmic reticulum (55,79). Sirtuins are a class of deacetylases composed of 7 protein members. Sirtuins distribution is cytosolic for SIRT2, mitochondrial for SIRT3-5 and nuclear for SIRT1, SIRT6-7 (54,55,90). Moreover, even if predominantly nuclear, SIRT1 is known to shuttle between nucleus and cytosol in response to stress conditions (46). As already described, sirtuins and PARPs govern a plethora of biological processes, for this reason a continuous re-synthesis of NAD^+ is necessary in each compartment. Localization of NBEs is still a matter of debate.

What is known is that the three isoforms of NMNATs are present in the nucleus (NMNAT1), in cytosol and Golgi apparatus (NMNAT2), and in mitochondria (NMNAT3)

(10,78,79). For NAMPT, NAPRT and NRK a predominant cytoplasmic localization was demonstrated, although controversial results supporting or contrasting a mitochondrial and nuclear localization were published over the years (17,27,47,69,104).

The knowledge of the physical and functional compartmentalization of these pathways is essential to tailor interventions that specifically alter NAD^+ levels in a desired cell type and compartment. For this reason, considering the potential of interfering with NAD^+ biosynthesis for cancer treatment, we decided to exploit genetically encoded biosensors to dissect the NAD^+ biosynthesis distribution in a model of metastatic melanoma.

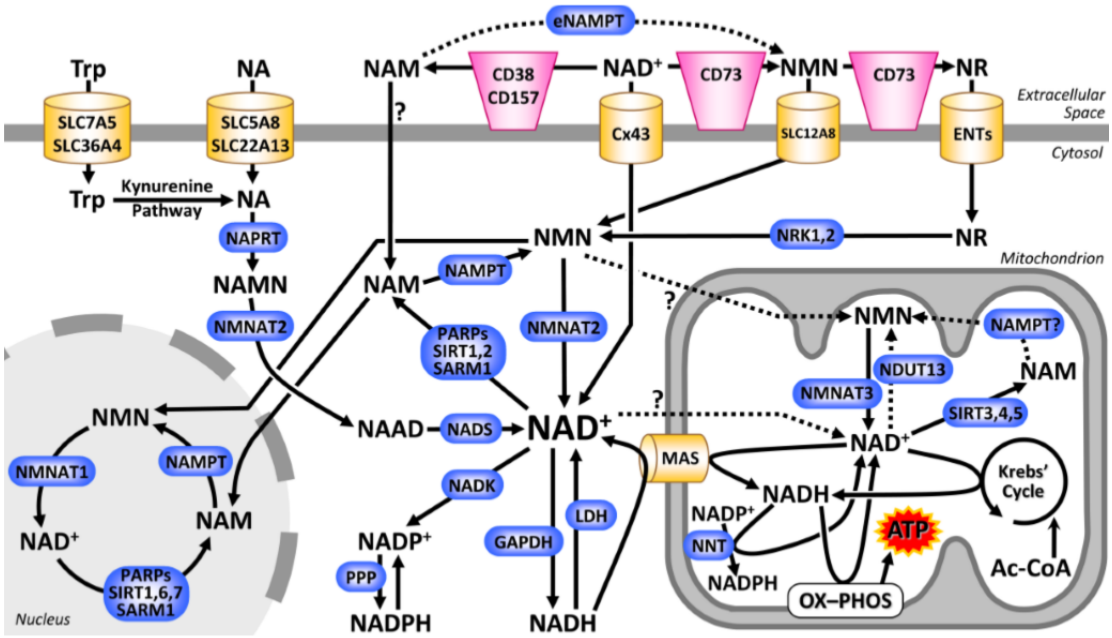

Figure 6. Compartmentation of NAD^+ biology.

The major routes for import, biosynthesis, and consumption of NAD+ in cytosol, nucleus and mitochondrion are shown. Dotted lines and question marks denote pathways for which limited evidence is available. *From Kulkarni et al., Antiox and Redox (2019).*

1.1.6 NAD^+ quantification: classic approaches and recent genetically encoded biosensors

Due to the centrality of NAD^+/NADH involving reactions, alterations of pyridine dinucleotide pools have a profound impact on cellular physiology and diseases development (50,70,87). In the past years, studies on NAD^+ metabolism, focused not only on the comprehension of NAD^+ production and function, but also on its subcellular distribution and on the possibility of a living and compartment-specific quantification of NAD^+ concentration. Traditional techniques available for NAD^+ detection are:

I. the enzymatic cycling assay: developed in 1961 by Lowry and colleagues, this method exerts an enzymatic cycling assay which first reduce NAD^+ to NADH. NADH is then oxidized back to NAD^+ in another reaction with the production of a colorimetric or fluorescent product. The rate of this final reduction assessed by the quantification of the fluorescent product, is proportional to the concentration of coenzyme in the system (61).

II. mass spectrometry: Fischer et al. 2004 developed a ^{13}C-constrained flux balancing analysis based on gas chromatography–mass spectrometry for NADH and NADPH detection (33).

III. high-performance liquid chromatography (HPLC): liquid chromatography-tandem mass spectrometric method that is sensitive and specific for simultaneous quantification of cellular NAD^+ and related compounds (107,115).

IV. capillary electrophoresis: this method coupled enzymatic cycling assay and capillary electrophoresis technology to determine the NAD^+ and NADH contents of a single cell (101).

V. isotope-labelling techniques: deuterium tracer approach that directly measures NADPH redox active hydrogen labelling (31).

However, in the last ten years, different fluorescence-based genetically encoded NAD^+ biosensors have been produced to overcome the main drawbacks of these traditional methods which essentially are i) the requirement of cell lysis and the incompatibility with live-cell quantification, ii) the ambiguity of the signal coming from the reduced or phosphorylated form of NAD^+, iii) the impossibility to distinguish signal coming from different subcellular compartments and iv) the necessity of an highly sophisticated technology (115).

Figure 7 summarizes all the genetically encoded biosensor for NAD^+ detection produced in the last decade for NAD^+ detection. Basically, these sensors are engineered proteins which couple specific binding properties (i.e. for NAD^+ alone) to a fluorescent chromophore. In this system, the substrate binding by the sensor induces a shift of the relative fluorescence intensity and/or spectra. Briefly, for the pyridine cofactor detection, the developed sensors are the NADH sensor Frex (114); the NAD^+/NADH ratio sensors Peredox (49), RexYFP (12), and SoNar (113), the NAD^+ sensor LigA-cpVenus (17), the $NADP^+$ sensors Apollo-$NADP^+$ (18) and NADPsor (111). Each of these sensors possess specific binding affinity for the substrate (NAD^+ or NADH or NAD^+/NADH ratio) which directly determine variability between sensors in the real amount of detectable NAD^+ or NAD^+/NADH ratio. Differences exist also in their intrinsic structural properties which render these sensors differentially stable, pH-sensitive or able of various grade of fluorescence change which ca be translated in the amplitude of signal transduction.

Finally, in 2018 Sallin and collaborators described a new class of semisynthetic fluorescent biosensors for measuring cellular free NAD^+ and NADPH/$NADP^+$ (85). This

sensor was described as a ratiometric tool excitable at long wavelengths (560 nm) with a large dynamic ranges and pH-insensitivity. It was designed according to the Snifit concept (15). Snifits contain an analyte-binding protein and two self-labeling protein tags (SNAP-tag) (53) and Halo-tag (60). In accordance with the fluorescence resonance energy transfer (FRET) technology analyte-binding affects the distance between the fluorophores resulting in FRET efficiency changes (Figure 8).

Considering all the described systems available for NAD^+ detection, we choose the cpVENUS based construct (Figure 9)(17) first for the specificity of the sensor for oxidized NAD^+ alone, secondly for the possibility to target the sensor in the different subcellular compartments (cytosol, mitochondria and nucleus), but also for its biochemical properties (reversible binding, K_{NAD^+}≈65µM) that make it suitable for physiological NAD^+ concentration. Nevertheless, the choice of this NAD^+ biosensor was due to its ratiometric properties and the easy and reproducible signal detection by cytofluorimetric measurements.

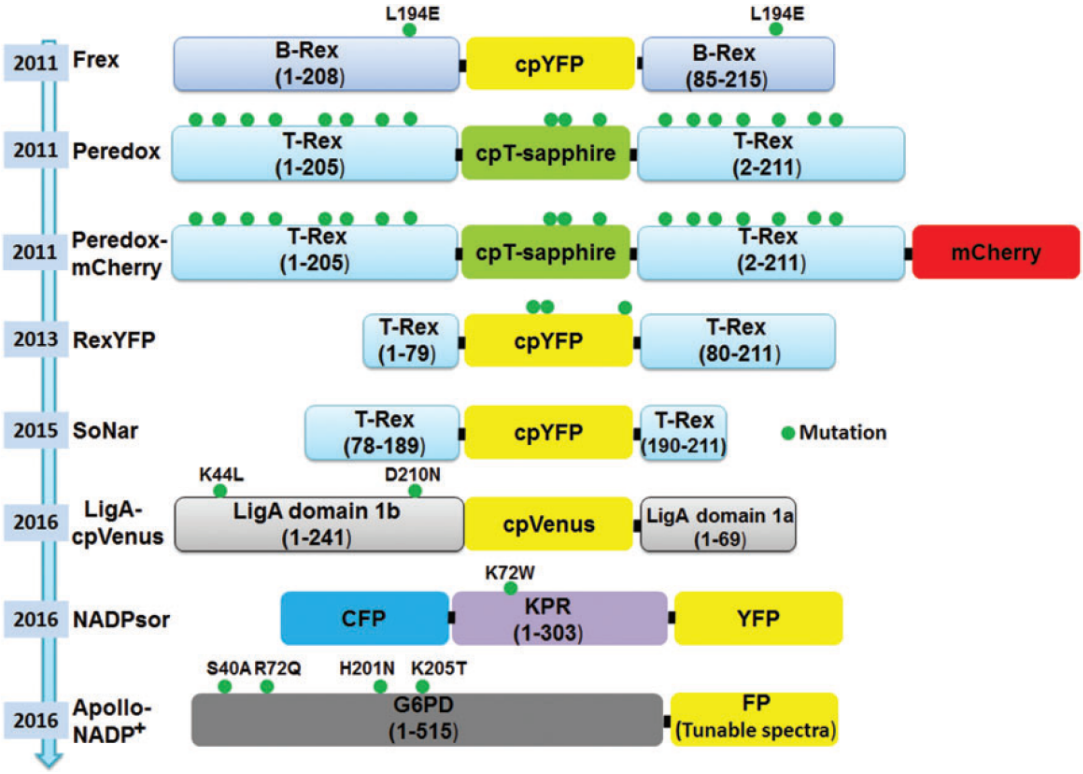

Figure 7. Schematic models of seven NAD^+/NADH and $NADP^+$/NADPH sensors.

Depicted are schematic diagrams for structure of $NAD(P)^+$/NAD(P)H sensors. Close circles in green indicate mutations in natural ligand-sensing domains and fluorescent proteins, which are genetically engineered to improve the fluorescent properties of sensors, such as responsiveness, selectivity, affinity, pH sensitivity, and brightness. *From Zhao et al., Antiox and Redox 2018, Review (115)*.

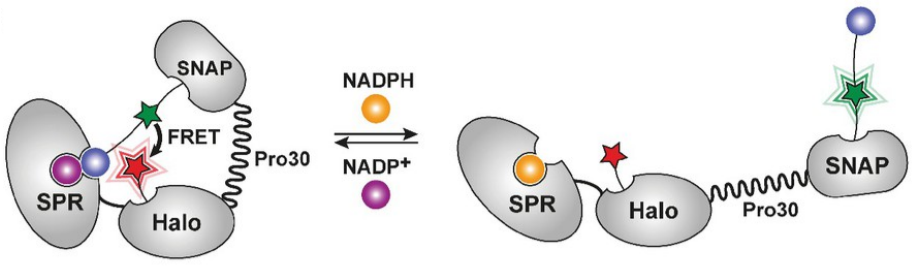

Figure 8. Design of semisynthetic sensors for NADP and NAD^+.

The fusion protein SPR-Halo-p30-SNAP is labeled via SNAP-tag with a synthetic molecule containing a FRET donor (green star) and a SPR inhibitor (blue ball, SMX), and via Halo-tag with a FRET acceptor. NADPH (orange ball) and NADP+ (purple ball) compete for the cofactor-binding site of SPR. The sensor can

monitor NADPH/NADP+ ratio changes by switching from a closed conformation to an open conformation, with high and low FRET efficiency, respectively. *From Sallin et al., eLIFE, (2019*) (85).

Figure 9. Structure of the cpVENUS based construct.

The bipartite NAD^+ binding domain of a bacterial DNA ligase (purple circles) is conjugated to a circularly permutated fluorescent Venus protein (green circle). Functionally, when NAD^+ is bound a change in the conformational structure of the sensor switches off the sensor fluorescence.

1.2 NAD^+ in cancer

Malignant transformation relies on metabolic reprogramming which consists in cellular metabolic adaptations aimed to satisfy new rates of growth and proliferation and to adapt to new microenvironment conditions such as oxygen and nutrient deficiency (3). It is called “metabolic rewiring” the multiple molecular mechanisms through which tumor cells feed new bioenergetics (rapid ATP generation) and biosynthetic needs (16). Activation of specific oncogenic pathways (i.e. RAS, BRAF, MEK driven pathways) are driver phenomenon targeting metabolic enzymes and downstream molecules, which leading to nucleoside deregulation, ensure tumor cell to overcome these unfavorable surroundings (3). Aerobic glycolysis is the energetic process through which tumor cells get their energy. In this context, NAD^+ can undoubtedly promote cancer proliferation by enhancing the glycolytic rate of the cell (22).

Indeed, the expression and the activity of NBEs are pivotal in these adaptations processes, because the quickly NAD^+ restoration is fundamental both for new energetic and signal transduction necessities of cancerous cells (3). Many studies reported that NAMPT is frequently over-expressed in hematological and solid tumors (37,63,88), and that there is a direct correlation between NAMPT expression and tumor stage, prognosis and survival. NAMPT is also often associated with enhanced acquired resistance to chemotherapeutic agents, increased steaminess and invasiveness properties of cancer cells (36) by regulating epithelial to mesenchymal transition (42,91). Also NAPRT was reported to be highly expressed in different types of cancer including ovarian and pancreatic cancer (74). Recently Li X. et al. showed a key role of both NAMPT and NAPRT in colon rectal cancer, revealing that the high

expression of NAMPT or NAPRT is associated with vascular invasion, advanced metastasis and adverse prognosis of patients. In this case, amplification of NAPRT gene and promoter methylation together with a miRNA-dependant regulation of NAMPT gene, correlate with activation of the TNF and PI3K-Akt signaling pathways (58).

Also NMNAT2 was reported to be over-expressed in colon rectal cancer, and its pharmacological inhibition enhanced tumour cell death (56).

Nevertheless, cancer initiation and progression are affected by intracellular levels of NAD^+ through the consequent modulation of NAD^+-consuming enzymes. As previously described in this thesis, PARPs mediate DNA repairing processes and chromatin stabilization, while sirtuins epigenetically modulate protein expression and activity. Both systems, fuelled in cancer cells by increased levels of NAD^+, activate several pro-cancer pathways involved in the first step of carcinogenesis and in the development of drug resistance as well (71,103). Among sirtuins, SIRT1 is known as a tumor-promoter protein. Indeed, downstream target of this deacetylase are an important tumor suppressor p53, and FOXO3a, a transcription factor emerged for its role in the cellular anti-oxidant system (52). NAD^+/NAMPT axis also regulates the pathways involved in the maintenance of cancer steaminess in colon cancers both in a SIRT1- and PARP1-dependent manner (103).

In addition, it is well known that the two main cellular NADases CD38 and CD73 are over-expressed in different types of cancer where they control activation of different signaling pathways and affect cancer immune tolerance (22,39). Importantly, It was recently reported that high expression of these NAD^+ consuming enzymes, sensitizes pancreatic cancer cells to chemical NAD^+ depletion (52).

Overall, these evidences suggested the idea of NAD^+ metabolism as a central core of energetic and transcriptional cancer cell adaptation mechanisms.

For these reasons, manipulation of these NAD^+-dependent mechanisms trough the depletion of NAD^+ levels, have been explored in many clinical trials and will be discussed in the following section.

1.2.1 Targeting NAD^+ metabolism in cancer

With the emerged key role of NADome in cancer initiation and progression, a lot of work has been done to develop drug able to reduce NAD^+ availability for tumors and inhibition of the main NAD^+ salvage pathways has been successful both *in vitro* and i*n vivo* treatments of different types of tumors (3,5,52). The main effects of targeting NAD^+ metabolism in cancer cells were: 1) the direct depletion of energy, 2) increase of ROS production, 2) inhibition of DNA repairing mechanism. As consequence, treated cells showed mitochondrial stress, cell cycle arrest, induction of apoptosis and autophagy processes.

Most of pharmacological attention was given to the inhibition of the main NAD^+ producing enzyme, NAMPT, with many NAMPT inhibitors (NAMPTis) which entered in clinical trials (3,52,103). In addition, a very recent paper described the synthesis of inhibitors able to discriminate between the intracellular and extracellular NAMPT (97), while others produced NAMPTis coupled with antibodies in order to increase safety and specificity of these compounds (51).

However NAMPTis, even if able to contain growth of advanced solid tumors, did not show tumor regression in four phase I clinical trials (103). Limitations in the use of NAMPTis are side effects, pharmacokinetics and compensatory mechanisms of NAD^+

production exerted by cancer cells. Activation of compensatory routes of NAD^+ production appears to be very tumor-specific and still represents a critical rock in the field of NAD-targeting therapy (24).

As an example of how NAPRT and NAMPT differential expression can be therapeutically explored was described in 2019 by Fons et al. (35). Fons and colleagues demonstrated that, in glioma, a truncated oncogene PPM1D, drives hypermetylation and promotes epigenetic silencing of NAPRT. Consequently, PPMD1 mutant cells were shown to be sensitive to NAMPT inhibition *in vivo* and *in vitro*, suggesting the NAMPT block as potential therapy of pediatric gliomas.

Table 1 summarizes recently reviewed modulators/inhibitors of the NADome with encouraging results obtained in animal model and human patients (3). As shown in the table, inhibitor of NAMPT and NAD^+ consuming enzymes as well, are more than promising therapeutic tools for the treatments of many types of tumors.

Future perspectives for tumor treatments are pointed to the development of combinatory strategies in which NAD^+ depletion synergies with oncogenic inhibitors or cytotoxic agents already used in cancer therapy.

Organelle-compartmentalization of NAD^+ biosynthesis and consumption cannot be underestimate in the design of therapies involving NAD^+ homeostasis. The idea behind this work is that, the biochemical characterization of NAD^+ biosynthesis in terms of tumor-specific expression patterns of NBEs and their subcellular distribution is a potential direction to improve efficacy of NBEs inhibition in cancer cells.

TABLE 1 | Pharmacologic tools currently undergoing pre- or clinical evaluation to block NADome enzymes.

Agent	Mechanism of action	Indication	Trial Stage
NAMPT INHIBITORS			
APO866 (FK866)	NAMPTi	T/IC	Clinical phase I
CHS-828 (GMX 1778)	NAMPTi	T/IC	Clinical phase I
GNE-617, GNE-618	NAMPTi	T	Pre-clinical
KPT-9274	Dual NAMPTi/PAX4i	T	Clinical phase I
OT-82	NAMPTi	T	Clinical phase I
Blocking antibody	eNAMPT neutralization	T/IC	Pre-clinical
CD38 INHIBITORS			
Daratumumab	Blocking antibody	MM/ALL	Clinical phase III
Isatuximab	Blocking antibody	MM	Clinical phase II-III
MOR202	Blocking antibody	MM	Clinical phase II
Apigenin	CD38i	MD	Pre-clinical
SIRTUINS INHIBITORS			
Cambinol	SIRT1/2i	T/ND	Pre-clinical
Sirtinol	SIRT1/2i	T/ND	Pre-clinical
Selermide	SIRT1/2i	T/ND	Pre-clinical
Tenovins	SIRT1i	T/ND	Pre-clinical
EX-527	SIRT1i	T/ND	Pre-clinical
Nicotinamide	SIRTi/NAD precursor	T/ND	Pre-clinical, phase I-II
IDO INHIBITORS			
Indoximod	IDOi	T	Clinical phase I-II
Epacadostat (INCB024360)	IDOi	T	Clinical phase II-III
Navoximod	IDOi	T	Clinical phase I
BMS-986205	IDOi	T	Clinical phase I-II

Table 1. I, inhibitor; T, solid and/or hematological tumors; IC, inflammatory conditions; MM, multiple myeloma; ALL, acute lymphoblastic leukemia; MD, metabolic diseases; ND, neurodegenerative diseases.

From Audrito et al., Frontiers in Immunology, Review (2019).

1.3 Metastatic melanoma (MM) as disease model

Malignant melanoma is the most common primary and aggressive neoplasm in adults and the sixth most prevalent cancer in the United States (6). Surgical treatment is often curative for localized stage I and stage II disease while the median survival for patients with distant metastases (stage IV melanoma) is less than 1 year (14). Melanomas show a high mutation burden and the most recurrent somatic mutations affect genes in key signaling pathways that govern proliferation (BRAF, NRAS and NF1), growth and metabolism (PTEN and KIT), resistance to apoptosis (TP53), cell cycle control (cyclin- dependent kinase inhibitor 2A (CDKN2A)) and replicative lifespan (telomerase reverse transcriptase (TERT)) (89).

Treatments of choice for melanoma patients consist of inhibitors of the v-Raf murine sarcoma viral oncogene homolog B (BRAF), an oncogene with activating mutation showed by almost 35-60% of patients (3). Frequently, the single base mutation at position 600 (V600E) of the oncogene leads to the over activation of BRAF-MEK-ERK axis and MAPK signaling (3,5). Through the over-activation of MAPK, BRAF mutations drive transcription of master regulators of metabolic responses, including hypoxia-inducible factor 1α (HIF-1α), MYC, microphthalmia-associated transcription factor (MITF), PGC1α, PI3K and STAT3 (73,93). The use of vemurafenib and dabrafenib, the agents that block MAPK signaling, in patients with melanoma and the BRAF V600E mutation, has been associated with prolonged and progression-free survival. However, MM patients treated with BRAFi show disease progression within 6 to 7 months after the initiation of treatment (34). This drug resistance is characterized by the reactivation of the MAPK pathway (5). To overcome this drug resistance and to improve antitumor activity, combination of immunotherapy with the BRAF targeted

therapy was suggested (48). Indeed, in 2011, the use of ipilimumab (a monoclonal antibody that blocks cytotoxic T lymphocyte antigen (CTLA)-4), nivolumab and pembrolizumab (two anti-programmed cell death-1 (PD-1)) were approved for patients with metastatic melanoma (77,95) and so far, the combinatorial approach of target therapy and immunotherapy have been very promising. However, some evidences of substantial liver toxicities together with the persistence of relapse and resistance episodes, prompts investigations into new of therapeutic strategies (29,48,77,95,112).

1.3.1 Metabolic reprogramming in MM: the role of NAD^+

The BRAF-mediated oncogenic signals are critical regulators of metabolic processes, by activating specific transcriptional programs. Specifically, by inducing rearrangement of transcription master regulators of metabolic responses (HIF-1α, MYC, MITF, PGC1α, PI3K and STAT3), BRAF dramatically drives metabolic reprogramming in melanoma cells, promotes aerobic glycolysis, actively represses OXPHOS and drastically increases tumor aggressiveness. It was shown that BRAFi/ MEKi treatment suppresses glucose metabolism (3,5), but the metabolic drug-resistant phenotype of treated patients is characterized by a reversion to mitochondrial respiration as an attempt to maintain ATP levels and escape cell death .

Due to the poor prognosis, the high frequency of chemo-resistance development and the necessity of new therapeutic opportunities, the combination of BRAFi/MEKi with agents targeting OXPHOS is a promising therapeutic strategy to overcome adaptive drug resistance (112).

A critical and indisputable role of NAD^+ metabolism in melanoma was reported (3,5,6,63,112). Our recent data showed that transformation of melanocytes to metastatic melanoma (MM) is accompanied by a net increase in global NAD^+ levels, particularly in the BRAF-mutated subset (5). Further elevation of NAD^+ levels occurs in cells that acquire resistance to BRAF inhibitors, an event accompanied by metabolic reprogramming and NAMPT over-expression (3,5,6,63). Over-expression of NAMPT was first demonstrated in 2012 by Maldi et al. in melanoma lesions compared to melanocytes (63), and confirmed in 2017 by Zhao et al. which observed increased NAMPT activity in the same tumor model (112). In this context, NAMPT overexpression is regulated at a transcriptional levels by NF-kB, STAT3, and HIF-1a, and the consequent increase in NAD^+ is needed to sustain cell proliferation and growth of MM cells, to improve cellular energetic performance and it may directly affect NAD^+ consumption pathways in an organelle-specific manner. In addition, the same authors demonstrated that NAMPT mediates the apoptosis resistance of melanoma cells through the NAMPT-E2F2-SIRT1 axis both in a NAD^+ dependent or independent ways (112). E2F2 is an important transcriptional factor with a well-known role in the NAD^+-dependent network (42).

Our group recently confirmed that the NAD^+ boost derived from NAMPT over-expression drives metabolic adaptation, observed after chronic exposure to BRAFi. The idea of NAMPT as a key determinant of the disease aggressiveness of BRAF-mutated melanomas was shown by observing that, the metabolic adaptation occurring in cell overexpressing NAMPT leads to the earlier development of BRAFi resistance, faster cellular growth, and a more efficient wounds repairing capacity. Furthermore, we found that treatment of melanoma cells with NAMPT inhibitors (NAMPTi) depleted NAD^+,

inducing mitochondrial stress, cell cycle arrest and apoptosis (5). Consistently, NAMPTis were highly effective in the treatment of melanoma xenografts, highlighting NAMPT as an actionable target for melanoma patients with BRAF mutations. Also in this case, NAMPT inhibition decreased proliferation and enhanced apoptosis of melanoma cells.

However, different processes determine the failure of NAMPTis, especially adverse side effects (thrombocytopenia, cardiotoxicity, retinopathy) (97), pharmacokinetics of the inhibitors and the over activation of others NAD^+ producing routes as compensatory mechanisms pursued by tumor cell to generate NAD^+ and to activate consecutive pathways (21,66,67). According to this concept, recently, Chowdhry et al. confirmed the addiction of melanoma cells on NAMPT enzymatic activity and showed that the tissue context and the genetic landscape of a tumor is the major determinant of dependence on specific NAD^+ metabolic pathway in cancer (24).

Aim of the work

Due to all the evidences concerning the complexity of NADome picture, we decided to put our attention on the understanding of NAD^+ biosynthesis compartmentalization and NAD^+ pool fluctuations in living melanoma cells with the final aim to compose the puzzle of NAD^+ biosynthesis in metastatic melanoma.

In this project, we studied NAD^+ bioavailability by dissecting the subcellular location of its biosynthesis. To the aim, we exploited a genetically-encoded fluorescent biosensor (17,25,30) to directly monitor free NAD^+ concentrations in subcellular compartments of MM cells and compartmentalized fluctuations of the cofactor under NAMPT inhibition or after treatments with precursors of all the aforementioned NAD^+ biosynthetic enzymes. Finally we connected this functional information to the biochemical evaluation of subcellular distribution of NAD^+ biosynthetic enzymes (NBEs) in order to identify new peculiar cancer weakness.

Innovation of the study

In this study we used genetically encoded NAD^+ biosensors to dynamically characterize subcellular NAD^+ biosynthesis in intact BRAF-mutated metastatic melanoma (MM) cells. The choice of this model derives from our previous studies showing that melanoma transformation is accompanied by dysregulation of NAD^+ biosynthesis, which may be therapeutically targeted. By using organelle specific biosensors, we monitored NAD^+ fluctuations in response to biosynthetic precursors or inhibitors. Together with subcellular localization data, these results offer a complete

picture of NAD^+ biosynthesis in MM cells and open the way to the use of biosensors to understand the NADome architecture in physio-pathological conditions.

The experimental approach pursued in this project, the obtained results and their discussion are described in detail in the attached research article which was accepted for publication in *Antioxidant and Redox Signaling* journal in August 2019.

Published Article

Original Research communication

Title: Subcellular characterization of NAD^+ biosynthesis in metastatic melanoma by using organelle-specific biosensors

Authors: Federica Gaudino[1], Ilaria Manfredonia[1], Antonella Managò[1], Valentina Audrito[1], Nadia Raffaelli[2], Tiziana Vaisitti[1], Silvia Deaglio[1].

Affiliations: [1]Department of Medical Sciences, University of Turin, Turin, 10126 Italy; [3]Department of Clinical Sciences and Department of Agricultural, Food and Environmental Sciences, Polytechnic University of Marche, Ancona, 60121 Italy.

Running head: Subcellular NAD^+ biosynthesis in melanoma

Corresponding author: Silvia Deaglio, MD, PhD, Department of Medical Sciences, University of Turin, via Nizza, 52, 10126 Torino, Italy. Phone: (+39-011) 670-9535. Email: silvia.deaglio@unito.it.

Keywords: NAD^+, BIOSENSOR, NAMPT, MELANOMA, METABOLISM.

Acknowledgements: This work was supported by the GILEAD Fellowship Program (Gilead Italia 2018 to SD) and by the Ministry of Education, University and Research, PRIN Project 2017CBNCYT (to SD) and "Dipartimenti di Eccellenza 2018–2022" (project #D1518000410001) to the Department of Medical Sciences of the University of Turin.

Abstract

Aim: NAD^+ plays central roles in a wide array of normal and pathological conditions. Inhibition of NAD^+ biosynthesis can be exploited therapeutically in cancer, including melanoma. To obtain quantitation of NAD^+ levels in live cells and to address the issue of the compartmentalization of NAD^+ biosynthesis, we exploited a recently described, genetically-encoded NAD^+ biosensor (LigA-cpVENUS), which was targeted to the cytosol, mitochondria and nuclei of BRAF-V600E A375 melanoma cells, a model of metastatic melanoma (MM).

Results: FK866, a specific inhibitor of nicotinamide phosphoribosyltransferase (NAMPT), the main NAD^+-producing enzyme in MM cells, was used to monitor NAD^+ depletion kinetics at the subcellular level in biosensor-transduced A375 cells. In addition, we treated FK866-blocked A375 cells with NAD^+ precursors, including nicotinamide, nicotinic acid, nicotinamide riboside and quinolinic acid, highlighting an organelle-specific capacity of each substrate to rescue from NAMPT block. Expression of NAD^+ biosynthetic enzymes was then biochemically studied in isolated organelles, revealing presence of NAMPT in all three cellular compartments, while NAPRT was predominantly cytosolic and mitochondrial, and NRK mitochondrial and nuclear. In keeping with biosensor data, QPRT was expressed at extremely low levels.

Innovation & Conclusions: Throughout this work, we validated the use of genetically encoded NAD^+ biosensors to characterize subcellular distribution of NAD^+ production routes in MM. The chance of real time monitoring of NAD^+ fluctuations after chemical perturbations, together with a deeper comprehension of the cofactor biosynthesis compartmentalization, strengthens the foundation for a targeted strategy of NAD^+ pool manipulation in cancer and metabolic diseases.

Introduction

Nicotinamide adenine dinucleotide (NAD^+) is a vital, ubiquitous and multifunctional cofactor regulating a wide range of biological processes (19,47). NAD^+ is essential as electron acceptor donor in glycolytic, tricarboxylic acid cycle (TCA) and oxidative phosphorylation redox reactions. The equilibrium existing between its oxidized (NAD^+) or reduced forms (NADH) mediates cellular antioxidation mechanisms, as well as cell redox state homeostasis, energy metabolism and mitochondrial functions (106). In addition, NAD^+ is the substrate of enzymes with fundamental roles in gene expression and cell signaling, independent of its redox properties. This large family of NAD^+ consuming enzymes includes adenosine diphosphate (ADP)-ribose transferases (ARTs) and poly ADP-ribose polymerases (PARPs), sirtuins (SIRTs) and cyclic ADP-ribose hydrolases (CD38/CD157) (44,98). Through their functional activities of post-translational modifications (ADP-ribosylation and deacetylation reactions), or by calcium signaling mobilization, these enzymes regulate gene transcription, cell differentiation, cell cycle progression, DNA repair, chromatin stability, among other biological processes (22), representing connecting elements between the metabolic state of a cell and its signaling and transcriptional activities.

The subcellular localization of specific biosynthetic pathways remains to be fully elucidated. Several efforts have been made to elucidate where NAD^+ biosynthesis occurs and whether there are exchanges between compartments (27,28,54,55,69,79). The maintenance of cellular NAD^+ pool is achieved through the re-oxidation from NADH or through the active synthesis of the pyridine nucleotide. Briefly, NAD^+ is synthesized through one *de novo* bio-synthetic pathway, starting from tryptophan/quinolinic acid (QA) and controlled by the enzyme quinolinate phosphoribosyltransferase (QPRT) (9,47) and three salvage pathways involving nicotinamide (NAM), nicotinic acid (NA), and

nicotinamide riboside (NR) (22,62). Each pathway is controlled by a rate-limiting enzyme, specifically nicotinamide phosphoribosyl transferase (NAMPT), nicotinate phosphoribosyltransferase (NAPRT) and nicotinamide riboside kinase (NRK). Among these pathways, the reaction controlled by NAMPT is the most relevant in mammalian cells (81), as the NAMPT substrate, NAM, is released by the main NAD^+ consuming enzymes, such as sirtuins and PARPs, connecting NAD^+ synthesis and degradation in a functional loop. NAMPT is frequently over-expressed in hematological and solid tumors (37,63,88). Our recent data showed that transformation of melanocytes to metastatic melanoma (MM) is accompanied by a net increase in global NAD^+ levels, particularly in the BRAF-mutated subset (5). Further elevation of NAD^+ levels occurs in cells that acquire resistance to BRAF inhibitors, an event accompanied by metabolic reprogramming and NAMPT overexpression (5,6). An increase in NAD^+ may be needed to sustain cell proliferation and growth of MM cells and it may directly affect NAD^+ consumption pathways in an organelle-specific manner.

Following this hypothesis, we studied NAD^+ bioavailability by dissecting the subcellular location of its biosynthesis. To the aim, we exploited a genetically-encoded fluorescent biosensor (17,25,30) to directly monitor free NAD^+ concentrations in subcellular compartments of MM cells and we connected this information to the biochemical evaluation of subcellular distribution of NAD^+ biosynthetic enzymes (NBEs).

Results

Generation of A375 cells stably expressing organelle-specific NAD^+ biosensor

To study the compartmentalization of NAD^+ biosynthesis, we used the BRAFV600E-mutated A375 cell line as a melanoma model. Both, BRAF inhibitor sensitive (S) and resistant (BiR) A375 were transduced with lentiviruses carrying the DNA coding for organelle-specific biosensor proteins (17). The biosensor contains an organelle specific sequence (as detailed in M&M), and the NAD^+-binding site of a bacterial DNA ligase (LigA1b-LigA1a). A cpVENUS fluorescent protein is connected to the bipartite NAD^+ binding domain of the enzyme. The structure allows biosensor fluorescence to be turned off when NAD^+ is bound. Based on their cpVENUS-fluorescence, transduced cells were flow-sorted to obtain stably expressing cells. Confocal microscopy shows the specificity of the biosensor in reaching the target compartment (Figure 1 A-B-C), as determined by co-localization of the biosensor signal (green) with the actin cytoskeleton (red), TOM20 (magenta) or DAPI (blue).

Organelle-specific effects of NAMPT inhibition

To study NAD^+-depletion kinetics induced by inhibiting the major mammalian NAD^+ biosynthetic pathway, we treated biosensor-encoding A375 cells with the well-known NAMPT inhibitor FK866 (5,66). The biosensor works by decreasing its fluorescence at 488 nm in the presence of increased levels of NAD^+, while its 405 nm fluorescence is unaffected by substrate variations and can be used to normalize the biosensor expression levels. Therefore, a decrease in NAD^+ levels leads to an increase of the 488 nm/405 nm fluorescence ratio (17,25,30). From previous works, it is known that FK866 treatment leads to a significant drop of total intracellular NAD^+ levels beginning few hours after treatment (43). Consistently, a time-lapse confocal microscopy analysis of A375 cells treated with FK866 (25nM), confirmed a net drop in cytosolic, mitochondrial and nuclear NAD^+ levels

steadily increasing over the 4 hours observation time (Figure 2A, movies 1-2-3). In order to obtain quantitative measurements, we then measured NAD^+ concentrations by cytofluorimetric analysis, at the fixed time point of 16 hours after FK866 treatment, when >90% of intracellular NAD^+ is depleted, according to previous data (17). In these conditions, we observed a sharp increase in the 488 nm/405 nm fluorescence ratio in FK886-treated cells in all the sub-cellular compartments (Figure 2B). The mean fluorescence ratio was augmented by 30±10% ($p=0.0002$), 38±14% ($p<0.0001$) and 32±9% ($p<0.0001$) in the cytosol, mitochondria and nuclei, respectively. Figure 2C is a representative example of the biosensor behavior under FK866 treatment. The dot plot on the left depicts changes in fluorescence at 488 nm in relation to 405 nm of cell expressing the biosensor or the cpVENUS only. No modification in the 488 nm fluorescence of the cpVENUS could be highlighted after treatment with FK866, confirming specificity of the results (relative histograms on the right).

Subcellular NAD^+ concentrations and effects of NMN on subcellular NAD^+ levels

In order to quantify NAD^+ fluctuations, we generated specific calibration curves for the cytosolic, the nuclear and the mitochondrial biosensors (Figure 3) (17,25,30). To do so, cells expressing cytosolic and nuclear biosensors were saponin-permeabilized to allow exogenous NAD^+ (used in a range of concentrations between 0 and 4 mM for cytosol and from 0 to 3mM for nucleus) to enter the cell or nucleus, as previously described (17). For the mitochondrial biosensor, saponin permeabilization was followed by rapid treatment with the ion channel-forming peptide alamethicin (AlaM), which renders mitochondria permeable to low-molecular-mass molecules (7,38,65). In this conditions, exogenous NAD^+ (from 0 to 10mM) entered in the organelle, inducing a linear reduction of the sensor fluorescence according to increasing NAD^+ concentrations. Table 1 shows fluorescence ratio 488 nm/405 nm calculations obtained from each biosensor and normalized on relative cpVENUS 488

nm/405 nm variations (for cytosolic and nuclear biosensors the mean of 4 replicates is shown, while 3 replicates are shown for mitochondrial biosensor). These cytofluorimetric measurements of fluorescence variations at each NAD^+ concentration were used to build specific sigmoidal curves. Lastly, by interpolating fluorescence ratio of non-permeabilized cells expressing the cytosolic biosensor to the relative titration curve, we found basal cytosolic mean values of NAD^+ in A375 cells of 261±74 M. The same experimental approach was used for the cells expressing the nuclear biosensor, detecting in this compartment a basal nuclear concentration of 259±85 M, while NAD^+ concentrations in the mitochondria were in the range of 499±154 M. Treatment with FK866 diminished cytosolic, nuclear and mitochondrial NAD^+ concentrations to values <0.7µM, below which the system is no longer sensitive. The amount of this NAD^+ depletion is in line with previously reported HPLC measurements of whole lysates from FK866-treated A375 cells (5).

Next, to further validate the system in our model, we studied the effects of nicotinamide mononucleotide (NMN), the product of the reaction catalyzed by NAMPT, on NAD^+ levels with or without treatment with FK866. After being produced by NAMPT, NMN is converted into NAD^+ by nicotinamide mononucleotide adenylyl-transferases (NMNATs), which are known to be expressed in the nucleus (NMNAT1), in the cytosol and Golgi (NMNAT-2) and in the mitochondria (NMNAT-3)(10,78,79). Therefore, we hypothesized that supplementation of NMN to cells could rescue NAD^+ levels in the presence of NAMPT inhibitors. As expected, treatment of A375 cells with NMN increased basal NAD^+ levels, in all cellular compartments and particularly in the cytosol (Figure 3C). After treating cells with the NMNAT substrate, we detected a consistent reduction of fluorescence ratio of 14±2% (p=0.001) in the cytosol corresponding to an increase in NAD^+ to 1621±606 M. In the nuclei, a reduction of fluorescence in the range of 8±4% (p=0.0037) corresponded to 651±280 M NAD^+. A

moderate but consistent fluorescence reduction of 9±3% (p=0.043) was also detected in mitochondria, where we measured an increase of the cofactor to a mean value of 2012±1855□M. Importantly, the combination of NMN and FK866, reverted the FK866-induced fluorescence ratio from 36±5% to 6±7% (p=0.01) in the cytosol, from 35±13% to 8±6% (p=0.002) in the mitochondria and from 28±7% to 16±8% (p=0.021) in the nuclei. The NMN-dependent rescue of NAMPT block is statistically significant when considering fluorescence ratios, and NAD^+ levels recover from <0.7□M to 167□M in cytosol, to 125□M in mitochondria and to 9□M into the nucleus.

Topography of NAD^+ Biosynthesis: NAM and NA primarily affect cytosolic NAD^+ levels

To obtain a complete topography of NAD^+ biosynthesis in MM, we then studied the efficacy of different NAD^+ precursors including NAM, NA, NR and QA, in sustaining NAD^+ biosynthesis and in rescuing from FK866-mediated NAD^+ depletion in the various compartments. We first treated cells with NAM and NA, substrates of the most relevant NAD^+ producing pathways in MM cells. NAM is recycled to NAD^+ in a two-step salvage pathway in which NAMPT, using the ribose-5-phosphate group of phosphoribosylpyrophosphate (PRPP) catalyzes a phosphoribosyl transferase reaction converting NAM to NMN (55). Treatment of cells with NAM led to a significant increase in cytosolic NAD^+ basal levels, as expected based on the documented cytosolic expression of NAMPT (5,27,69) (Figure 4A). In fact, in this compartment, the fluorescence ratio was reduced by 17±7% (p=0.004), corresponding to an increase in basal NAD^+ levels to 1930±980□M. A slighter decrease in the fluorescence ratio was observed in the nuclei, where we measured an increase in basal levels of the cofactor to 489±195□M, whereas no changes were measured in mitochondria. An additional mechanism leading to NAD^+ accumulation could be linked to block of NAD^+ intracellular consumption, as NAM is a

powerful noncompetitive inhibitor of NAD^+-consuming enzymes (SIRTs and PARPs) (13,55,86). Consistently, even when added to A375 cells treated with FK866, NAM was able to partially prevent NAD^+ loss. In fact, in the cytosol, we observed a rescue from FK866-induced NAD^+ depletion, with fluorescence ratios going from 29±14% to 15±13% (p=0.02, NAD^+ concentration of 36□M), in mitochondria from 46±20% to 14±20% (p=0.005), while in the nuclear compartment from 37±6% to 23±8% (p=0.003). The observed NAM-driven rescue of NAD^+ levels, would essentially reflect the inhibition of sirtuin activities in the three compartments, while in the nuclei PARPs activity block could also contribute to the outcome.

NA is the substrate of NAPRT, which converts NA into nicotinic acid mononucleotide (NAMN) via the Press-Handler pathway (20,47). NA was effective in the cytosol, as well in nuclei and mitochondria, both in increasing compartmentalized NAD^+ basal levels and in countering the effects of NAMPT inhibition (Figure 4B). The highest NA-dependent increase in basal NAD^+ was detected in the cytosol (13±4% of fluorescence ratio reduction, p=0.013, NAD^+ concentration of 976±550□M), followed by mitochondria (1031±550□M). The evidence of a NA/NAPRT-mediated rescue from FK866-induced NAD^+ depletion, confirms the reported finding that NAPRT-mediated NAD^+ production limits the action of NAMPT inhibitors used in cancer treatment (74,90).

Topography of NAD^+ Biosynthesis: NR and QA showed an organelle-specific impact on NAD^+ levels

We then tested the effects of NR and QA on subcellular NAD^+ levels. NR is an additional salvageable NAD^+ precursor via the NRKs-mediated pathway. NR conversion to NAD^+ is initiated by phosphorylation of NR to NMN by NR kinases (NRKs) (80,96). Studying the subcellular capacity of NR in sustaining NAD^+ production in MM, we found NR to be effective in increasing basal NAD^+ levels in cytosol (760±557□M) and in nuclei (533±166□M) (Figure

5A). However, NR was able to counter the effects of FK866 predominantly in nuclei (from 27±5% to 19±5% p=0.0004) and in mitochondria (from 37±12% to 14±11% p=0.007) (Figure 5A). In mitochondria of cells supplemented with NR and treated with FK866, NAD^+ levels were kept between 50-240□M, thus preventing its drop after FK866 exposure. Lastly, treatment of A375 with QA, an intermediate precursor of the 8 steps-*de novo* synthesis pathway, increased NAD^+ levels only in mitochondria. Furthermore, QA offered partial and weak protection from FK866-induced NAD^+ depletion selectively in mitochrondria (Figure 5B). This finding is in line with the reported low expression of QPRT in MM (5,47).Together, these results support the idea of a dominant NAD^+ production via the recycling pathways in MM cells, with a clear preference for the cytosolic NAM-NAMPT. In the cytosol NAPRT can be considered a second active NAD^+ producer, while in the organelles, NRK appears to play a key role as NAD^+ biosynthetic enzyme.

Subcellular localization of NAD^+ biosynthetic enzymes

Subcellular distribution of NBEs remains an incompletely understood aspect of NAD^+ physiology, with increasing evidence suggesting that NAD^+ biosynthesis is compartmentalized in a cellular- and tissue-dependent way (27,79). To determine the subcellular expression pattern of NBEs in A375 cells in exponential growth phase and to interpret data obtained with the organelle-specific biosensors, we used confocal microscopy and biochemical analyses. Western blot analyses were performed on cytosol and isolated mitochondria and nuclei. Confocal microscopy was used to support biochemical analysis. By comparing expression levels of the four NBEs, we confirmed that NAMPT is the dominant NBEs (Figure 6A-C, left panel). We then dissected NBEs subcellular localization by looking at protein distribution in the separate compartments. A percentage of expression for the different compartments was determined by dividing pixel intensity of the specific bands

pertaining to a given compartment by the sum of the pixel intensities of the bands pertaining to all compartments. Western blot analysis showed that NAMPT is mostly cytosolic (84.16% of localization, Figure 6A), with low mitochondrial (10.74%) and nuclear (5.1%) expression. Organelles purity was confirmed by using specific markers (anti-Vinculin, -tubulin,-actin antibodies specifically highlight cytosolic fraction; anti-hadha and –cytochrome C antibodies identify mitochondrial enrichment while anti-H2A antibody was used for nuclear compartment detection). NAPRT was essentially cytosolic (92.2%), with minor fractions present in mitochondria (5.7%) and nuclei (2.1%). Conversely, NRK was mostly mitochondrial (67.2%) and nuclear (32.7%). QPRT was detectable at very low levels only in cytosol and in mitochondria (not shown). Organelle purity was confirmed by using specific markers. NBEs subcellular distribution was confirmed by confocal microscopy, by using organelle-specific markers and a software co-localization tool (Figure 6C, right panel). The panel on the left shows the overlay of the NBE under analysis and the compartment specific marker. The three panels on the right show expression of the NBE under analysis in the indicated compartment.

Proof-of-principle of the use of the biosensor to monitor NAD^+ levels

Lastly, we decided to use the biosensor to compare NAD^+ levels in A375 cells before (S) and after the acquisition of resistance to BRAF inhibitors (BiR). These cellular models offered us a strategic and clinically relevant example of cancer metabolic adaptation suitable for characterization of NAD^+ biosynthesis. In keeping with our prior data showing that A375/BiR cells are characterized by higher expression of NAMPT and constitutive higher levels of NAD^+ (5), the biosensors showed a more pronounced sensitivity to NAD^+-depletion through NAMPT inhibition. Specifically, as evidenced by a higher fluorescence variations, upon FK866 treatment, A375/BiR cells were more severely NAD^+-depleted than /S variants, at least in the

cytosol and nucleus (Figure 7). These results, not only confirm that NAMPT is the master regulator of NAD^+ biosynthesis in A375/BiR cells, but also evidence a compartmentalized response to NAMPT inhibition in the two cell lines. Specifically, a highly significant difference in response to FK866 was highlighted in the cytosol and the nuclei, while no significant difference was observed in mitochondria. This result is consistent with the literature suggesting a differential behavior of mitochondria compared to the cytosol or the nuclei in the dynamics of metabolites exchange (69,90). In addition, we found that, in A375, the most mitochondrial expressed NBE is NRK, potentially explaining the lower sensitivity of A375/BiR mitochondria to NAMPT inhibition.

Overall, these data validate NAD^+ biosensors as tools to understand whether the main pathways responsible for NAD^+ production differ across subcellular compartments or under chemical perturbations.

Discussion

Because of its essential role and ubiquitous presence, alterations of NAD^+ concentrations are associated with a large number of pathological conditions, including metabolic diseases like obesity, diabetes and insulin resistance, inflammation and immune responses (26,79,110). A decrease in NAD^+ levels is also a hallmark of aging and aging-associated pathologies, such as neurodegeneration and motor function decline. For these reasons, NAD^+ boosting molecules or inhibitors of the NADases received remarkable attention as antiaging agents or co-adjuvants for maintaining NAD^+ homeostasis (79). On the other hand, a significant branch of research on NAD^+ metabolism documented increased levels of the cofactor during tumorigenesis (5,88), thus rendering NAD^+ metabolism an attractive therapeutic target in cancer treatment. Inhibitors against NAMPT, the major intracellular NBE, are under development for phase I and II clinical trials for patients with ovarian, pancreatic and rectal cancers or with hematological malignancies, including multiple myeloma and chronic lymphocytic leukemia (45,99,102). Even if some clinical responses were observed, patients treated with NAMPT inhibitors experienced significant toxicity, including thrombocytopenia and gastrointestinal complications. The modest success of FK866 in cancer patients, may be explained by the activation of rescue pathways that can overcome NAMPT block and restore NAD^+ levels through alternative routes. Most important in this context is NAPRT, the rate-limiting enzyme in the metabolism of dietary NA into NAD^+. Epigenetic regulation of NAPRT leads to gene silencing in some tumors, while in the cases in which it is over-expressed, the enzyme is responsible for the failure of NAMPTi-based treatments (20,74). Like NA, NR can be introduced through diet, but it is also the by-product of extracellular NMN dephosphorylation reaction carried out by CD73 (90), an ectoenzyme involved in the generation of adenosine, in turn a powerful immunosuppressant. Recent

reports indicate that NR, via NRK activity, maintains cancer NAD^+ homeostasis in the presence of NAMPTi, contributing to treatment failure (24,41,90). In addition,

the dynamic NAD^+/NADH balance impacts on the redox state of cancer cells. In fact, tumors possess higher levels of reactive oxygen species (ROS), rendering them more sensitive to changes in the redox status (23,59). In this context, NAD(H)/NADP(H) balance regulates glutathione reductase (GR) and thioredoxin reductase (TR) activities, major components of the antioxidant defense system (40,68,100). Specifically, reducing equivalents from NADPH are used to regenerate reduced glutathione (GSH) from the oxidized form (GSSG), fueling the ROS scavenging system of the cell (100). For this reason, the availability of NAD^+ precursors and their subcellular-specific employment could regulate the activity of GSH/GSSG system in an organelle-dependent way. The prevalence of a cytosolic GSH pool likely makes it sensitive to the presence of an active NAM/NAMPT axis and to its pharmacological inhibition. In addition, G6PD, which is the major source of NADPH, can also be activated post-transcriptionally by SIRT2 dependent deacetylation (100).

Characterization of subcellular NAD^+ pools and compartmentalized NAD^+ biosynthetic pathways are pivotal in order to tailor therapeutic interventions, modulating the balance between NAD^+ consumption and production. This work was undertaken with the dual aim of obtaining a clearer picture of NAD^+ biosynthesis in BRAF-mutated melanoma cells and to set-up conditions to follow its modifications in live cells. To address our aims, out of all the tools developed in the last 10 years for real time measuring of NAD^+ or NAD^+/NADH levels (85,115), we used a recently devised genetically-encoded NAD^+ biosensor (17), which was targeted to the cytosol, nuclei and mitochondria. The choice of this biosensor is based on its intrinsic properties I) as a ratiometric tool specific for NAD^+ detection, II) optimal binding

affinity for physiological cellular NAD^+ concentrations. In addition, III) the biosensor is easy to manipulate and has equally easy readouts.

BRAF-V600E A375 cells were used as experimental model, as it was shown that, in order to support increased cellular growth rates, they reprogrammed NAD^+ biosynthesis by overexpressing NAMPT. This NAMPT overexpression is even stronger during BRAF inhibitors resistance development (5,6), a frequent clinical complication incurring in metastatic melanoma of patients. The basal NAD^+ concentration in the cytosol and nuclei of A375 cells in the exponential growth phase was estimated at 260µM and at 499µM in mitochondria (Figure 8), in keeping with previously reported values for total intracellular free NAD^+ levels ranging between 200 and 500µM (19,47,55,98,104). In addition, in basal conditions, the recently estimated NAD^+ pool concentrations in cultured mammals and murine derived cell lines (HEK293T, HeLa, U2OS, NIH3T3) move from 60µM to 120µM for nuclei and cytosol (17,47,85), increasing to ~300µM in mitochondria (17,19,47). These reported compartmentalized NAD^+ concentrations are tightly dependent on the cell type. For this reason, it was not surprising for us to find the aforementioned concentration of free NAD^+ in cytosol, nuclei and mitochondria of A375 cells. Indeed, for these cells, HPLC measurements already detected more than double the NAD^+ content compared to normal melanocytes (5). Moreover, by combining dynamic measurements using live cells and organelle fractionation, we can conclude that NAMPT is quantitatively the most expressed NAD biosynthetic enzyme in A375 cells and undoubtedly the dominant one in the cytosol (Figure 8). If we look at the nuclear compartment, the prevalent NBE is NRK followed by NAMPT. Cytosol and nuclei are considered exchangeable compartments for the diffusion of NAD^+ pools (55). This concept, together with the revealed high expression levels of NRK in nuclei, could explain similar levels of NAD^+ concentrations between cytosol and nucleus of A375. By combining two well

established protocols for mitochondria purification (36,57,108), we found that mitochondria of MM cells appear to be equipped predominantly with NRK and possibly with lower levels of NAMPT and NAPRT (Figure 8). Even though mitochondrial NAD^+ contents can reach up to 70% of total intracellular NAD^+ (1), how its levels are maintained remains a matter of debate. Two processes, glycolysis and NAD^+ biosynthesis, directly link cytoplasmic and mitochondrial NAD^+ pools (92). The NADH produced by glycolysis is transported into the mitochondrial matrix by NAD/NADH redox shuttles (106), providing reducing equivalents for the TCA cycle and electron transport chain (ETC). The former process reduces O_2 to water and NADH to NAD^+ in order to produce ATP, generating mitochondrial NAD^+ levels much higher than the other cellular compartment (75). In addition, maintenance of NAD^+ levels in the compartment is also dependent on salvaging NAM produced by NAD^+-consuming enzymes. The current view of the field is that NRKs are preferentially located in the cytosol and nucleoplasm, and while it is accepted that NR is the preferred NAD^+ precursor for mitochondrial NAD^+ synthesis (47,69,90), no evidence is available indicating NRK activity in mitocondria. One of the current hypotheses about mitochondrial NAD^+ is that, it can be maintained by the NMNAT3 conversion of NMN or by the membrane transport of NAD^+ precursors (NAM, NMN) or even NAD^+ itself. Indeed, while some demonstrated that NAD^+ is unable to cross the mitochondrial membrane and that pyridine nucleotides are instead broken down to the corresponding nucleosides (69,76,90,92), others affirmed that only intact NAD^+ can restore depleted mitochondria NAD^+ levels (27,32). Even if the first eukaryotic mitochondrial NAD^+ carrier, named Ndt1p, was identified in *Saccharomyces cerevisiae* (94) and in 2009 Palmieri et al. identified a chloroplast and mitochondrial NAD^+ carrier protein in *Arabidopsis thaliana* (72), no mammalian transporter for NAD^+ has yet been found. For these reasons, whether there is a complete NAD^+ biosynthetic apparatus or

a system transport for NAD^+ in mitochondria remains unclear (27). Our data, both biochemical and biosensor based, suggest that NRK is present in the mitochondria, at least in A375 melanoma cells, arguing in favor of direct NAD^+ biosynthesis in these organelles. In addition, the prevalent NRK expression in mitochondria, could suggest the use of NRK inhibitors. Consistently, recent data by Chowdhry et al. indicated that NRK-dependent synthesis of NAD^+ causes the failure of NAMPTis and that both NRK knockdown or dual inhibition of NAMPT and NRK lowered the dose of FK866 needed to arrest tumour growth, leading to persistent tumor regression *in vivo* (24).

Intracellular NAMPT is ubiquitously present in human body, even if its expression varies according to tissues (79,82). Different experimental approaches have been exploited to define mitochondrial presence of NAMPT in different cell lines with controversial results (17,27,47,69,104). We found that also mitochondria are sensitive to NAMPT inhibition and that a small amount of NAMPT is present in these organelles. However, alternative explanations, such as cytosolic import of NAD^+ cannot be excluded, as well as a cell type dependence of NAD^+ biosynthetic pathways localization. At the concentrations used, NA raised NAD^+ levels rescued FK866-dependent NAD^+ depletion in all compartments, pointing to a very efficient NAPRT pathway. On the contrary, neither NR nor NAM raised NAD^+ levels in mitochondria even though both NRK and NAMPT are present in the organelles. The finding that NMN induced a slight increase of mitochondrial NAD^+ may reflect regulated transport of these metabolites. With the exception of QA, all tested NAD^+ precursors, including NMN, are effective in boosting NAD^+ levels in cytosol and nuclei. Among them, only NR is unable to rescue the FK866-induced NAD^+ depletion in cytosol, in keeping with previous data that suggest that the NAM and NR pathways can both converge on NAMPT. According to these data, NR would be converted to NAM by a nucleoside phosphorylase

prior to the NAMPT catalyzed reaction (8,64). This is in keeping with the very low levels of NR kinase in the cytosol, as demonstrated by western blot and confocal microscopy.

Overall, our data provide a proof-of-principle of the validity of the use of organelle-specific biosensors to monitor NAD^+ fluctuations that occur in physio-pathological conditions. They also reinforce the concept of compartmentalization of NAD^+ biosynthesis, an essential aspect to understand how NAD^+ metabolism impacts on cancer cell metabolic adaptation. By offering a more complete picture of NAD^+ biosynthesis in MM, we aim to open the window of therapeutic strategies combining inhibitors of oncogenic signaling and of NAD^+ biosynthesis.

Materials and Methods

CpVenus-based NAD^+ sensor construct

The NAD^+ biosensor is a chimeric molecule, composed by a circularly permutated Venus (cpVenus) fluorescent protein linked to a bipartite NAD^+-binding domain of a bacterial DNA ligase (LigA1b and LigA1a) (17,25,30). Cytosolic, nuclear and mitochondrial biosensor expression vectors were kindly provided by X.A. Cambronne (Department of Molecular Biosciences, University of Texas, Austin, USA).

The incorporation of specific targeting sequences (CTGCAGAAAAAGCTGGAAGAGCTGGAACTGGAC for cytosol, ATGCTGGCCACCCGCGTGTTCAGCCTGGTGGGCAAGCGCGCCATCAGCACCAGCGTGTGCGT GCGCGCCCAC for mitochondria, and CCAAAGAAGAAGCGTAAGGTA for nuclei), allows these biosensors to be expressed in an organelle-specific way. DNA was amplified, incorporated in lentiviral particles (see below) and used for stable cell transduction. The LigA-cpVENUS biosensor presents two excitation peaks, one at 488 nm that decreases according to NAD^+ elevation and a second one at 405 nm that is unaffected by substrate variations, serving as internal control and system calibrator (17,25,30).

Generation of lentivirus

The vector plasmids (CMV-Sensor-IRES-puro-5 µg) together with third generation packaging plasmids (pMDL-2µg, pRSV-Rev-2µg, and the VSVG envelope encoding plasmid-1.2 µg, all from Addgene) were used for 293T cells transfection by using commercial Effectene transfection system (Quiagen, Milan, Italy, cod. 301425). After 48h, supernatants were collected, cells debris excluded (centrifugation at 600 x g for 5 minutes), and lentiviral particles concentrated (ultracentrifugation at 121,603 g for two hours) and used for cell transduction.

Generation of cell lines stably expressing biosensors

A375 BRAFV600E-mutated cell lines were from the American Type Culture Collection (ATCC). BRAFi-resistant (BiR) variants were generated as described (5). Cells expressing cytosolic, nuclear or mitochondrial biosensors were obtained by transducing both A375/sensitive (S) and /BiR cells with a lentiviral vector carrying the specific organelle-targetable biosensor or with the organelle-targetable cpVENUS alone, using polybrene (8ug/ml; Sigma, Milan, Italy, cod. H9268). cpVENUS positive cells were flow sorted (FACSAriaIII, BD Biosciences, Milan, Italy) and used as reported.

Cell treatments

A375/S and /BiR lines were cultured in RPMI-1640 (Sigma, cod. R6504) with 10% of fetal calf serum (FCS) (Sigma, cod. F7524) and 10 IU/ml of penicillin / streptomycin (Sigma, cod. P4333). Cells were exposed to the following treatments for 16 hours. For NAMPT inhibition, cells were treated with 25 nM FK866 (Sigma, cod. F8557). Treatments with NAD^+ precursors were with 500 µM NMN (cod. N3501), 6 µM NA (cod. N4126), 0.5 µM NAM (cod. N3376), 200 µM QA (cod. P63204 all from Sigma) and 100 µM NR (kind gift of ChromaDex, Irvine, CA).

Flow cytometry analysis

For flow cytometry analysis, cells were trypsinized (Sigma, cod. T4049) and collected in RPMI 10% FCS. Sensor/cpVenus FITC (excitation 488 nm, emission 530/30 nm) and BV510 (excitation 405 nm, emission 525/50 nm) were measured by flow cytometry (BD FACS Celesta) and data processed with DIVA version 8 (BD Biosciences) and FlowJo version 10.01 softwares (TreeStar, Ashland, OR). Cells were gated using forward scatter (FSC) and side scatter (SSC) for the live cells and then further gated on both SSC and FSC width to exclude doublets, analyzing at least 10^4 cells / sample. The analysis required a

double ratio, expressed as a "ratio of ratios" (i.e. fold change). The first is the ratiometric 488/405 measurement detected by the biosensor, the second one is obtained by the parallel analysis of 488 nm/405 nm fluorescence changes of cells expressing the cpVENUS-only control (17,25,30). The cpVENUS 488/405 nm fluorescence ratio is used to normalize for NAD^+ changes independent of the biosensor. F0 refers to the ratio of ratios obtained in untreated conditions (F0=1). NAD^+ variations are finally expressed as the inverse relationship between the "ratio of ratios" changes and the cofactor concentrations. A "ratio of ratios" value >1 indicates decresed NAD^+ concentrations, while values <1 indicate increased levels of NAD^+.

Calibration curves

Calibration curves of cytosolic and nuclear biosensors were generated as previously described (17). In details, cells expressing correspondent biosensors were permeabilized with saponin (0.005%), in the presence of propidium iodide (PI)(Sigma cod.P4170). Permeabilization status was monitored by looking at the percentage of PI positive cells. For mitochondrial biosensor-expressing cells, cells were first permeabilized for 10 minutes with saponin 0.005% and then treated with alamethicin (Sigma, cod. A4665) 30ug/ml in order to obtain mitochondria permeabilization and NAD^+ exchange trough the organelle. Permeabilized cells were exposed to increasing concentrations (from 0 to 4 mM for cytosol and nuclei and from 0 to 10 mM for mitochondria) of exogenous NAD^+ (Sigma, cod. N-1511-1G). The NAD^+-dependent fluorescence changes were monitored by flow cytometry. Each point composing the curve is the result of the ratio between 488nm and 405nm values of the biosensor normalized to the relative cpVENUS and lastly normalized on F0 (0 μM of NAD^+).

Mitochondria purification

Mitochondria isolation was performed as previously described (36,57,108). Briefly, A375 cells ($15x10^7$) cells were resuspended in IB_C buffer (200mM sucrose, 1mM Tris-HCL, 1 mM EGTA, pH 7.4). Cells were mechanically disrupted by using an Elvehjem potter (Sigma, cod. P7734), and suspension was centrifuged (600 x g, 10 min, 4°C). This step was repeated twice to increase purification efficiency. Pellet was discarded and mitochondria-containing supernatant was centrifuged (8,000 x g, 10 min, 4°C). A centrifugation (8,500 x g, 10min, 4°C) on a discontinuous Percoll gradient (60, 30 and 18% Percoll, GE Healthcare, Milan, Italy, cod. GE17-0891-01), in IBc buffer, was used as last step of purification. The fraction between the 30% and 18% gradients was collected and washed three times by centrifugation at 19,000 x g for 10 min. Purified mitochondria were then lysed in a 1% NP-40 based buffer, subjected to Bradford quantification and prepared for western blot analysis with the same technical approach used for whole cell lysates (see below).

Nuclei purification

Nuclei were isolated through a salt-based protocol and differential centrifugation steps. Cells ($8x10^6$) were collected from culture and resuspended in Buffer A (300 mM Sucrose, 10 mM Hepes, 10 mM KCl, 2 mM $MgCl_2$, 1 mM EGTA, KOH pH 7.9, complete of phosphatase and protease inhibitors). To lyse cells, NP-40 (0,15%) was added to the suspension, before centrifuging (1300 x g, 5 min) and the supernatant was centrifuged (16000 g, 15 min, 4C°) to eliminate membrane residues and used as cytosolic portion of the fractionating protocol. The pellet was then washed 5x in Buffer B (50 mM Hepes, 400 mM NaCl, 1 mM EDTA, pH 7.5 NAOH) (1300 g, 5 min) and subjected to 5 sonication

steps. Finally, the suspension was centrifuged (130000 g for 15 min) and the obtained supernatant used as pure nuclear protein fraction.

Western blot analysis

Whole cells or subcellular fractions obtained as described above, were resolved by SDS-PAGE, and transferred to nitrocellulose filter membranes (Biorad, Milan, cod. 1704158) (5). After blocking (5% Not-fat dry milk, Santa Cruz Biotechnology, Heidelberg, Germany, cod. sc2325), membranes were incubated with: anti-GFP (Cell Signaling Technologies, Danvers, MA, cod 2555S), anti-vinculin (Abcam, Cambridge, UK, cod. 130007), -tubulin (Cell Signaling Technologies, cod.2114), -actin (Santa Cruz Biotechnology, cod. sc-47778), -Hadha (Abcam, cod. 203114), -cytochrome C (BD Bioscience, cod. 556433), -H2A (Abcam, cod. ab18255), anti-NAMPT (Bethyl Laboratories, Montgomery, TX A300-779A), anti-NAPRT1 (Novus Biologicals, Cambridge, UK, cod. NBP1-87243), anti-C9orf95 (NRK1, ab169548) and anti-QPRT (ab57125 both from Abcam). After incubation with horseradish peroxidase-conjugated secondary antibody (PerkinElmer, Milan, Italy, cod. NEF822001EA), reaction was visualized with ECL (Biorad, cod. 1705061) using ImageQuant LAS4000 (GE Healthcare, Milan, Italy).

Confocal microscopy

Cells expressing organelle-specific biosensors were cultured on glass cover slips in 24-well plates, rinsed once with PBS, fixed (4% PFA, 10 minutes, room temperature), permeabilized (0.1% saponin in PBS, 20 minutes, room temperature) and saturated with pre-immune goat serum (1:100, 1 hour, 4 °C). For NBEs localization studies, after saturation cells were incubated with primary antibodies: anti-NAMPT, anti-NAPRT1, anti-C9orf95 and anti-QPRT, anti-TOM20 (cod. SC-11415 from Santa Cruz Biotechnology). MitoTracker Deep Red (ThermoFischer, cod. M22426). was used for

mitochondria staining. TCS SP5 laser scanning confocal microscope equipped with an oil immersion 63X objective, was used for fluorescence acquisition. Images were acquired with LAS AF software (Leica Microsystem), files were processed with Photoshop (Adobe Systems, San Jose, CA) and pixel intensity was calculated using the ImageJ software (http://rsbweb.nih.gov/ij/).

Time lapse analysis

For time lapse imaging, A375 ($12X10^5$) were cultured into a μ-Slide 4 well Ibidi Chambered coverslips (Ibidi, Giemme Snc, Milan, Italy, cod. 80426), in RPMI-1640 with 10% of FCS. TCS SP5 was also equipped for maintaining cells under physiological conditions (5% CO_2 and 37°C). for the duration of the experiments. At time 0 (t=0) cells were treated with FK866 25 nM, for a period of 6 hours. Time lapse series were acquired with 10 minutes intervals for mitochondrial and nuclear biosensor, for 5 minutes for cytosolic biosensor, between successive frames. To obtain the full cell thickness, for each acquisition field, different z-stacks were acquired and the sum of z stacks obtained with ImageJ software analysis was used for video generation. Finally, the ImageJ plugin ''image calculator'' was used to obtain the values of fluorescence ratio between 488nm and 405nm channels.

Statistical analysis

Statistical analyses were performed with GraphPad version 6.0 (GraphPad Software Inc., La Jolla, CA). Data were analyzed by two-sided paired Student's t test. Results are reported as box plots, where the top and bottom margins of the box define the 25th and 75th percentiles, the line in the box defines the median, and the error bars define the minimum and maximum of all data. *P value*<.05 was considered to be statistically significant.

Results

Generation of A375 cells stably expressing organelle-specific NAD^+ biosensor

To study the compartmentalization of NAD^+ biosynthesis, we used the BRAFV600E-mutated A375 cell line as a melanoma model. Both, BRAF inhibitor sensitive (S) and resistant (BiR) A375 were transduced with lentiviruses carrying the DNA coding for organelle-specific biosensor proteins (17). The biosensor contains an organelle specific sequence (as detailed in M&M), and the NAD^+-binding site of a bacterial DNA ligase (LigA1b-LigA1a). A cpVENUS fluorescent protein is connected to the bipartite NAD^+ binding domain of the enzyme. The structure allows biosensor fluorescence to be turned off when NAD^+ is bound. Based on their cpVENUS-fluorescence, transduced cells were flow-sorted to obtain stably expressing cells. Confocal microscopy shows the specificity of the biosensor in reaching the target compartment (Figure 4 A-B-C), as determined by co-localization of the biosensor signal (green) with the actin cytoskeleton (red), TOM20 (magenta) or DAPI (blue).

Organelle-specific effects of NAMPT inhibition

To study NAD^+-depletion kinetics induced by inhibiting the major mammalian NAD^+ biosynthetic pathway, we treated biosensor-encoding A375 cells with the well-known NAMPT inhibitor FK866 (5,66). The biosensor works by decreasing its fluorescence at 488 nm in the presence of increased levels of NAD^+, while its 405 nm fluorescence is unaffected by substrate variations and can be used to normalize the biosensor expression levels. Therefore, a decrease in NAD^+ levels leads to an increase of the 488 nm/405 nm fluorescence ratio (17,25,30). From previous works, it is known that FK866 treatment leads to a significant drop of total intracellular NAD^+ levels beginning few

hours after treatment (43). Consistently, a time-lapse confocal microscopy analysis of A375 cells treated with FK866 (25nM), confirmed a net drop in cytosolic, mitochondrial and nuclear NAD^+ levels steadily increasing over the 4 hours observation time (Figure 5A, movies 1-2-3). In order to obtain quantitative measurements, we then measured NAD^+ concentrations by cytofluorimetric analysis, at the fixed time point of 16 hours after FK866 treatment, when >90% of intracellular NAD^+ is depleted, according to previous data (17). In these conditions, we observed a sharp increase in the 488 nm/405 nm fluorescence ratio in FK886-treated cells in all the sub-cellular compartments (Figure 5B). The mean fluorescence ratio was augmented by 30±10% ($p=0.0002$), 38±14% ($p<0.0001$) and 32±9% ($p<0.0001$) in the cytosol, mitochondria and nuclei, respectively. Figure 5C is a representative example of the biosensor behavior under FK866 treatment. The dot plot on the left depicts changes in fluorescence at 488 nm in relation to 405 nm of cell expressing the biosensor or the cpVENUS only. No modification in the 488 nm fluorescence of the cpVENUS could be highlighted after treatment with FK866, confirming specificity of the results (relative histograms on the right).

Subcellular NAD^+ concentrations and effects of NMN on subcellular NAD^+ levels

In order to quantify NAD^+ fluctuations, we generated specific calibration curves for the cytosolic, the nuclear and the mitochondrial biosensors (Figure 6) (17,25,30). To do so, cells expressing cytosolic and nuclear biosensors were saponin-permeabilized to allow exogenous NAD^+ (used in a range of concentrations between 0 and 4 mM for cytosol and from 0 to 3mM for nucleus) to enter the cell or nucleus, as previously described (17). For the mitochondrial biosensor, saponin permeabilization was followed by rapid treatment with the ion channel-forming peptide alamethicin (AlaM), which renders mitochondria permeable to low-molecular-mass molecules (7,38,65). In this

conditions, exogenous NAD^+ (from 0 to 10mM) entered in the organelle, inducing a linear reduction of the sensor fluorescence according to increasing NAD^+ concentrations. Table 1 shows fluorescence ratio 488 nm/405 nm calculations obtained from each biosensor and normalized on relative cpVENUS 488 nm/405 nm variations (for cytosolic and nuclear biosensors the mean of 4 replicates is shown, while 3 replicates are shown for mitochondrial biosensor). These cytofluorimetric measurements of fluorescence variations at each NAD^+ concentration were used to build specific sigmoidal curves. Lastly, by interpolating fluorescence ratio of non-permeabilized cells expressing the cytosolic biosensor to the relative titration curve, we found basal cytosolic mean values of NAD^+ in A375 cells of 261±74µM. The same experimental approach was used for the cells expressing the nuclear biosensor, detecting in this compartment a basal nuclear concentration of 259±85µM, while NAD^+ concentrations in the mitochondria were in the range of 499±154µM. Treatment with FK866 diminished cytosolic, nuclear and mitochondrial NAD^+ concentrations to values <0.7µM, below which the system is no longer sensitive. The amount of this NAD^+ depletion is in line with previously reported HPLC measurements of whole lysates from FK866-treated A375 cells (5).

Next, to further validate the system in our model, we studied the effects of nicotinamide mononucleotide (NMN), the product of the reaction catalyzed by NAMPT, on NAD^+ levels with or without treatment with FK866. After being produced by NAMPT, NMN is converted into NAD^+ by nicotinamide mononucleotide adenylyl-transferases (NMNATs), which are known to be expressed in the nucleus (NMNAT1), in the cytosol and Golgi (NMNAT-2) and in the mitochondria (NMNAT-3)(10,78,79). Therefore, we hypothesized an NMN-driven rescue of NAD^+ levels upon NAMPT chemical inhibition. As expected, treatment of A375 cells with NMN increased basal NAD^+ levels, in all cellular

compartments and particularly in the cytosol (Figure 6C). After treating cells with the NMNAT substrate, we detected a consistent reduction of fluorescence ratio of 14±2% (p=0.001) in the cytosol corresponding to an increase in NAD^+ to 1621±606μM. In the nuclei, a reduction of fluorescence in the range of 8±4% (p=0.0037) corresponded to 651±280μM NAD^+. A moderate but consistent fluorescence reduction of 9±3% (p=0.043) was also detected in mitochondria, where we measured an increase of the cofactor to a mean value of 2012±1855μM. Importantly, the combination of NMN and FK866, reverted the FK866-induced fluorescence ratio from 36±5% to 6±7% (p=0.01) in the cytosol, from 35±13% to 8±6% (p=0.002) in the mitochondria and from 28±7% to 16±8% (p=0.021) in the nuclei. The NMN-dependent rescue of NAMPT block is statistically significant when considering fluorescence ratios, and NAD^+ levels recover from <0.7μM to 167μM in cytosol, to 125μM in mitochondria and to 9μM into the nucleus.

Topography of NAD^+ Biosynthesis: NAM and NA primarily affect cytosolic NAD^+ levels

To obtain a complete topography of NAD^+ biosynthesis in MM, we then studied the efficacy of different NAD^+ precursors including NAM, NA, NR and QA, in sustaining NAD^+ biosynthesis and in rescuing from FK866-mediated NAD^+ depletion in the various compartments. We first treated cells with NAM and NA, substrates of the most relevant NAD^+ producing pathways in MM cells. NAM is recycled to NAD^+ in a two-step salvage pathway in which NAMPT, using the ribose-5-phosphate group of phosphoribosylpyrophosphate (PRPP) catalyzes a phosphoribosyl transferase reaction converting NAM to NMN (55). Treatment of cells with NAM led to a significant increase in cytosolic NAD^+ basal levels, as expected based on the documented cytosolic expression of NAMPT (5,27,69) (Figure 7A). In fact, in this compartment, the fluorescence ratio was reduced by 17±7% (p=0.004), corresponding to an increase in

basal NAD^+ levels to 1930±980μM. A slighter decrease in the fluorescence ratio was observed in the nuclei, where we measured an increase in basal levels of the cofactor to 489±195μM, whereas no changes were measured in mitochondria. An additional mechanism leading to NAD^+ accumulation could be linked to block of NAD^+ intracellular consumption, as NAM is a powerful noncompetitive inhibitor of NAD^+-consuming enzymes (SIRTs and PARPs) (13,55,86). Consistently, even when added to A375 cells treated with FK866, NAM was able to partially prevent NAD^+ loss. In fact, in the cytosol, we observed a rescue from FK866-induced NAD^+ depletion, with fluorescence ratios going from 29±14% to 15±13% (p=0.02, NAD^+ concentration of 36μM), in mitochondria from 46±20% to 14±20% (p=0.005), while in the nuclear compartment from 37±6% to 23±8% (p=0.003). The observed NAM-driven rescue of NAD^+ levels, would essentially reflect the inhibition of sirtuin activities in the three compartments, while in the nuclei PARPs activity block could also contribute to the outcome.

NA is the substrate of NAPRT, which converts NA into nicotinic acid mononucleotide (NAMN) via the Press-Handler pathway (20,47). NA was effective in the cytosol, as well in nuclei and mitochondria, both in increasing compartmentalized NAD^+ basal levels and in countering the effects of NAMPT inhibition (Figure 7B). The highest NA-dependent increase in basal NAD^+ was detected in the cytosol (13±4% of fluorescence ratio reduction, p=0.013, NAD^+ concentration of 976±550μM), followed by mitochondria (1031±550μM). The evidence of a NA/NAPRT-mediated rescue from FK866-induced NAD^+ depletion, confirms the reported finding that NAPRT-mediated NAD^+ production limits the action of NAMPT inhibitors used in cancer treatment (74,90).

Topography of NAD^+ Biosynthesis: NR and QA showed an organelle-specific impact on NAD^+ levels

We then tested the effects of NR and QA on subcellular NAD^+ levels. NR is an additional salvageable NAD^+ precursor via the NRKs-mediated pathway. NR conversion to NAD^+ is initiated by phosphorylation of NR to NMN by NR kinases (NRKs) (80,96). Studying the subcellular capacity of NR in sustaining NAD^+ production in MM, we found NR to be effective in increasing basal NAD^+ levels in cytosol (760±557µM) and in nuclei (533±166 M) (Figure 8A). However, NR was able to counter the effects of FK866 predominantly in nuclei (from 27±5% to 19±5% p=0.0004) and in mitochondria (from 37±12% to 14±11% p=0.007) (Figure 8A). In the latter, NR preserved NAD^+ levels between 50-240µM, thus preventing its drop after FK866 exposure. Treatment of A375 with QA, an intermediate precursor of the 8 steps-*de novo* synthesis pathway starting from tryptophan, increased NAD^+ levels only in mitochondria. Furthermore, selectively in these organelles, it offered partial and weak protection from FK866-induced NAD^+ depletion (Figure 8B). This finding is in line with the reported low expression of QPRT in MM (5,47).Together, these results support the idea of a dominant NAD^+ production via the recycling pathways in MM cells, with a clear preference for the cytosolic NAM-NAMPT. In the cytosol NAPRT can be considered a second active NAD^+ producer, while in the organelles, NRK appears to play a key role as NAD^+ biosynthetic enzyme.

Subcellular localization of NAD^+ biosynthetic enzymes

Subcellular distribution of NBEs remains an incompletely understood aspect of NAD^+ physiology, with increasing evidence suggesting that NAD^+ biosynthesis is compartmentalized in a cellular- and tissue-dependent way (27,79). To determine the subcellular expression pattern of NBEs in A375 cells in exponential growth phase and to

interpret data obtained with the organelle-specific biosensors, we used confocal microscopy and biochemical analyses. Western blot analyses were performed on cytosol and isolated mitochondria and nuclei. Confocal microscopy was used to support biochemical analysis. By comparing expression levels of the four NBEs, we confirmed that NAMPT is the dominant NBEs (Figure 9A-C, left panel). We then dissected NBEs subcellular localization by looking at protein distribution in the separate compartments. A percentage of expression for the different compartments was determined by dividing pixel intensity of the specific bands pertaining to a given compartment by the sum of the pixel intensities of the bands pertaining to all compartments. Western blot analysis showed that NAMPT is mostly cytosolic (84.16% of localization, Figure 9A), with low mitochondrial (10.74%) and nuclear (5.1%) expression. Organelles purity was confirmed by using specific markers (anti-Vinculin, -tubulin,-actin antibodies specifically highlight cytosolic fraction; anti-hadha and –cytochrome C antibodies identify mitochondrial enrichment while anti-H2A antibody was used for nuclear compartment detection). NAPRT was essentially cytosolic (92.2%), with minor fractions present in mitochondria (5.7%) and nuclei (2.1%). Conversely, NRK was mostly mitochondrial (67.2%) and nuclear (32.7%). QPRT was detectable at very low levels only in cytosol and in mitochondria (not shown). Organelle purity was confirmed by using specific markers. NBEs subcellular distribution was confirmed by confocal microscopy, by using organelle-specific markers and a software co-localization tool (Figure 9C, right panel). The panel on the left shows the overlay of the NBE under analysis and the compartment specific marker. The three panels on the right show expression of the NBE under analysis in the indicated compartment.

Proof-of-principle of the use of the biosensor to monitor NAD^+ levels

Lastly, we decided to use the biosensor to compare NAD^+ levels in A375 cells before (S) and after the acquisition of resistance to BRAF inhibitors (BiR). These cellular models offered us a strategic and clinically relevant example of cancer metabolic adaptation suitable for characterization of NAD^+ biosynthesis. In keeping with our prior data showing that A375/BiR cells are characterized by higher expression of NAMPT and constitutive higher levels of NAD^+ (5), the biosensors showed a more pronounced sensitivity to NAD^+-depletion through NAMPT inhibition. Specifically, as evidenced by a higher fluorescence variations, upon FK866 treatment, A375/BiR cells were more severely NAD^+-depleted than /S variants, at least in the cytosol and nucleus (Figure 10). These results, not only confirm that NAMPT is the master regulator of NAD^+ biosynthesis in A375/BiR cells, but also evidence a compartmentalized response to NAMPT inhibition in the two cell lines. Specifically, a highly significant difference in response to FK866 was highlighted in the cytosol and the nuclei, while no significant difference was observed in mitochondria. This result is in keeping with literature suggesting a differential behavior of mitochondria compared to the cytosol or the nuclei in the dynamics of metabolites exchange (69,90) and with our data indicating that NAMPT is mostly a cytosolic enzyme. In addition, we found that, in A375, the most mitochondrial expressed NBE is NRK, potentially explaining the lower sensitivity of A375/BiR mitochondria to NAMPT inhibition.

Overall, these data validate NAD^+ biosensors as tools to understand whether the main pathways responsible for NAD^+ production differ across subcellular compartments or under chemical perturbations.

Discussion

Because of its essential role and ubiquitous presence, alterations of NAD^+ concentrations are associated with a large number of pathological conditions, including metabolic diseases like obesity, diabetes and insulin resistance, inflammation and immune responses (26,79,110). A decrease in NAD^+ levels is also a hallmark of aging and aging-associated pathologies, such as neurodegeneration and motor function decline. For these reasons, NAD^+ boosting molecules or inhibitors of the NADases received remarkable attention as antiaging agents or co-adjuvants for maintaining NAD^+ homeostasis (79). On the other hand, a significant branch of research on NAD^+ metabolism documented increased levels of the cofactor during tumorigenesis (5,88), thus rendering NAD^+ metabolism an attractive therapeutic target in cancer treatment. Inhibitors against NAMPT, the major intracellular NBE, are under development for phase I and II clinical trials for patients with ovarian, pancreatic and rectal cancers or with hematological malignancies, including multiple myeloma and chronic lymphocytic leukemia (45,99,102). Even if promising, initial trials have shown limited clinical responses, also because they were burdened by significant thrombocytopenia and gastrointestinal toxicity. The modest success of FK866 in cancer patients, may be explained by the activation of rescue pathways that can overcome NAMPT block and restore NAD^+ levels through alternative routes. Most important in this context is NAPRT, the rate-limiting enzyme in the metabolism of dietary NA into NAD^+. Epigenetic regulation of NAPRT leads to gene silencing in some tumors, while in the cases in which it is over-expressed, the enzyme is responsible for the failure of NAMPTi-based treatments (20,74). Like NA, NR can be introduced through diet, but it is also the by-product of extracellular NMN dephosphorylation reaction carried out by CD73 (90), an

ectoenzyme involved in the generation of adenosine, in turn a powerful immunosuppressant. Recent reports indicate that NR, via NRK activity, maintains cancer NAD^+ homeostasis in the presence of NAMPTi, contributing to treatment failure (24,41,90). In addition,

the dynamic NAD^+/NADH balance impacts on the redox state of cancer cells. In fact, tumors possess higher levels of reactive oxygen species (ROS), rendering them more sensitive to changes in the redox status (23,59). In this context, NAD(H)/NADP(H) balance regulates glutathione reductase (GR) and thioredoxin reductase (TR) activities, major components of the antioxidant defense system (40,68,100). Specifically, reducing equivalents from NADPH are used to regenerate reduced glutathione (GSH) from the oxidized form (GSSG), fueling the ROS scavenging system of the cell (100). For this reason, the availability of NAD^+ precursors and their subcellular-specific employment could regulate the activity of GSH/GSSG system in an organelle-dependent way. The prevalence of a cytosolic GSH pool likely makes it sensitive to the presence of an active NAM/NAMPT axis and to its pharmacological inhibition. In addition, G6PD, which is the major source of NADPH, can also be activated post-transcriptionally by SIRT2 dependent deacetylation (100).

Characterization of subcellular NAD^+ pools and compartmentalized NAD^+ biosynthetic pathways are pivotal in order to tailor therapeutic interventions, modulating the balance between NAD^+ consumption and production. This work was undertaken with the dual aim of obtaining a clearer picture of NAD^+ biosynthesis in BRAF-mutated melanoma cells and to set-up conditions to follow its modifications in live cells. To address our aims, out of all the tools developed in the last 10 years for real time measuring of NAD^+ or NAD^+/NADH levels (85,115), we used a recently devised

genetically-encoded NAD^+ biosensor (17), which was targeted to the cytosol, nuclei and mitochondria. The choice of this biosensor is based on its intrinsic properties I) as a ratiometric tool specific for NAD^+ detection, II) optimal binding affinity for physiological cellular NAD^+ concentrations. In addition, III) the biosensor is easy to manipulate and has equally easy readouts.

BRAF-V600E A375 cells were used as experimental model, as it was shown that, in order to support increased cellular growth rates, they reprogram NAD^+ biosynthesis by overexpressing NAMPT. This NAMPT overexpression is even stronger during BRAF inhibitors resistance development (5,6), a frequent clinical complication incurring in metastatic melanoma of patients. The basal NAD^+ concentration in the cytosol and nuclei of A375 cells in the exponential growth phase was estimated at 260µM and at 499µM in mitochondria (Figure 11), in keeping with previously reported values for total intracellular free NAD^+ levels ranging between 200 and 500µM (19,47,55,98,104). In addition, in basal conditions, the recently estimated NAD^+ pool concentrations in cultured mammals and murine derived cell lines (HEK293T, HeLa, U2OS, NIH3T3) move from 60µM to 120µM for nuclei and cytosol (17,47,85), increasing to ~300µM in mitochondria (17,19,47). These reported compartmentalized NAD^+ concentrations are tightly dependent on the cell type. For this reason, it was not surprising for us to find the aforementioned concentration of free NAD^+ in cytosol, nuclei and mitochondria of A375 cells. Indeed, for these cells, HPLC measurements already detected more than the double of NAD^+ content compared to normal melanocytes (5). Moreover, by combining dynamic measurements using live cells and organelle fractionation, we can conclude that NAMPT is quantitatively the most expressed NAD biosynthetic enzyme in A375 cells and undoubtedly the dominant one in the cytosol (Figure 11). If we look at the nuclear

compartment, the prevalent NBE is NRK followed by NAMPT. Cytosol and nuclei are considered exchangeable compartments for the diffusion of NAD^+ pools (55). This concept, together with the revealed high expression levels of NRK in nuclei, could explain similar levels of NAD^+ concentrations between cytosol and nucleus of A375. By combining two well established protocols for mitochondria purification (36,57,108), we found that mitochondria of MM cells appear to be equipped predominantly with NRK and possibly with lower levels of NAMPT and NAPRT (Figure 11). Even though mitochondrial NAD^+ contents can reach up to 70% of total intracellular NAD^+ (1), how its levels are maintained remains a matter of debate. Two processes, glycolysis and NAD^+ biosynthesis, directly link cytoplasmic and mitochondrial NAD^+ pools (92). The NADH produced by glycolysis is transported into the mitochondrial matrix by NAD/NADH redox shuttles (106), providing reducing equivalents for the TCA cycle and electron transport chain (ETC). The former process reduces O_2 to water and NADH to NAD^+ in order to produce ATP, generating mitochondrial NAD^+ levels much higher than the other cellular compartment (75). In addition, maintenance of NAD^+ levels in the compartment is also dependent on salvaging NAM produced by NAD^+-consuming enzymes. The current view of the field is that NRKs are preferentially located in cytosol and nucleoplasm, and while it is accepted that NR is the preferred NAD^+ precursor for mitochondrial NAD^+ synthesis (47,69,90), no evidence is available indicating NRK activity in this organelle. One of the current hypotheses about mitochondrial NAD^+ is that, it can be maintained by the NMNAT3 conversion of NMN or by the membrane transport of NAD^+ precursors (NAM, NMN) or even NAD^+ itself. Indeed, while some demonstrated that NAD^+ is unable to cross the mitochondrial membrane and that pyridine nucleotides are instead broken down to the corresponding nucleosides (69,76,90,92), others affirmed that only intact

NAD^+ can restore depleted mitochondria NAD^+ levels (27,32). Even if the first eukaryotic mitochondrial NAD^+ carrier, named Ndt1p, was identified in *Saccharomyces cerevisiae* (94) and in 2009 Palmieri et al. identified a chloroplast and mitochondrial NAD^+ carrier protein in *Arabidopsis thaliana* (72), no mammalian transporter for NAD^+ has yet been found. For these reasons, whether there is a complete NAD^+ biosynthetic apparatus or a system transport for NAD^+ in mitochondria remains unclear (27). Our data, both biochemical and biosensor based, suggest that NRK is present in the mitochondria, at least in A375 melanoma cells, arguing in favor of direct NAD^+ biosynthesis in these organelles. Moreover, this prevalent NRK expression in mitochondria, could suggest the use of NRK inhibitors. Chowdhry et al. recently dissected the molecular mechanisms and the genetic landscape driving NAD^+ synthesis pathway choice by tumors. They found that NRK-dependent synthesis of NAD^+, as result of enhancer amplification, causes the failure of NAMPTis and that both NRK knockdown or dual inhibition of NAMPT and NRK lowered FK866 dose needed to arrest tumour growth, leading to persistent tumor regression in vivo (24).

Intracellular NAMPT is ubiquitously present in human body, even if its expression varies according to tissues (79,82). Different experimental approaches have been exploited to define mitochondrial presence of NAMPT in different cell lines with controversial results (17,27,47,69,104). We found that also mitochondria are sensitive to NAMPT inhibition and that a small amount of NAMPT is present in these organelles: however, we cannot exclude the cytosolic import of NAD^+, a possible enzyme translocation mechanism or a cell type dependence of NAD^+ biosynthetic pathways localization. At the concentrations used, NA was able to raise NAD^+ and to rescue FK866-dependent NAD^+ depletion in all compartments, pointing to a very efficient NAPRT pathway. At the concentrations used,

neither NR nor NAM raised NAD^+ levels in mitochondria even though both NRK and NAMPT are present, while NMN induced a slight increase of mitochondrial NAD^+, possibly reflecting regulated transport of these metabolites. With the exception of QA, all tested NAD^+ precursors, including NMN, are effective in boosting NAD^+ levels in cytosol and nuclei. Among them, only NR is unable to rescue the FK866-induced NAD^+ depletion in cytosol, which might suggest that in this compartment the NR >>NAD^+ pathway is NAMPT-dependent rather than NRK-dependent. This implies conversion of NR to NAM by a nucleoside phosphorylase prior to the NAMPT catalyzed reaction (8,64). This is in keeping with the very low levels of NR kinase in the cytosol, as demonstrated by western blot and confocal microscopy.

Overall, our data provide a proof-of-principle of the validity of the use of organelle-specific biosensors to monitor NAD^+ fluctuations occurring in physio-pathological conditions. They also reinforce the concept of compartmentalization of NAD^+ biosynthesis, an essential aspect to understand how NAD^+ metabolism impacts on cancer cell metabolic adaptation. By offering a more complete picture of NAD^+ biosynthesis in MM, we aim to open the window of therapeutic strategies combining inhibitors of oncogenic signaling and of NAD^+ biosynthesis.

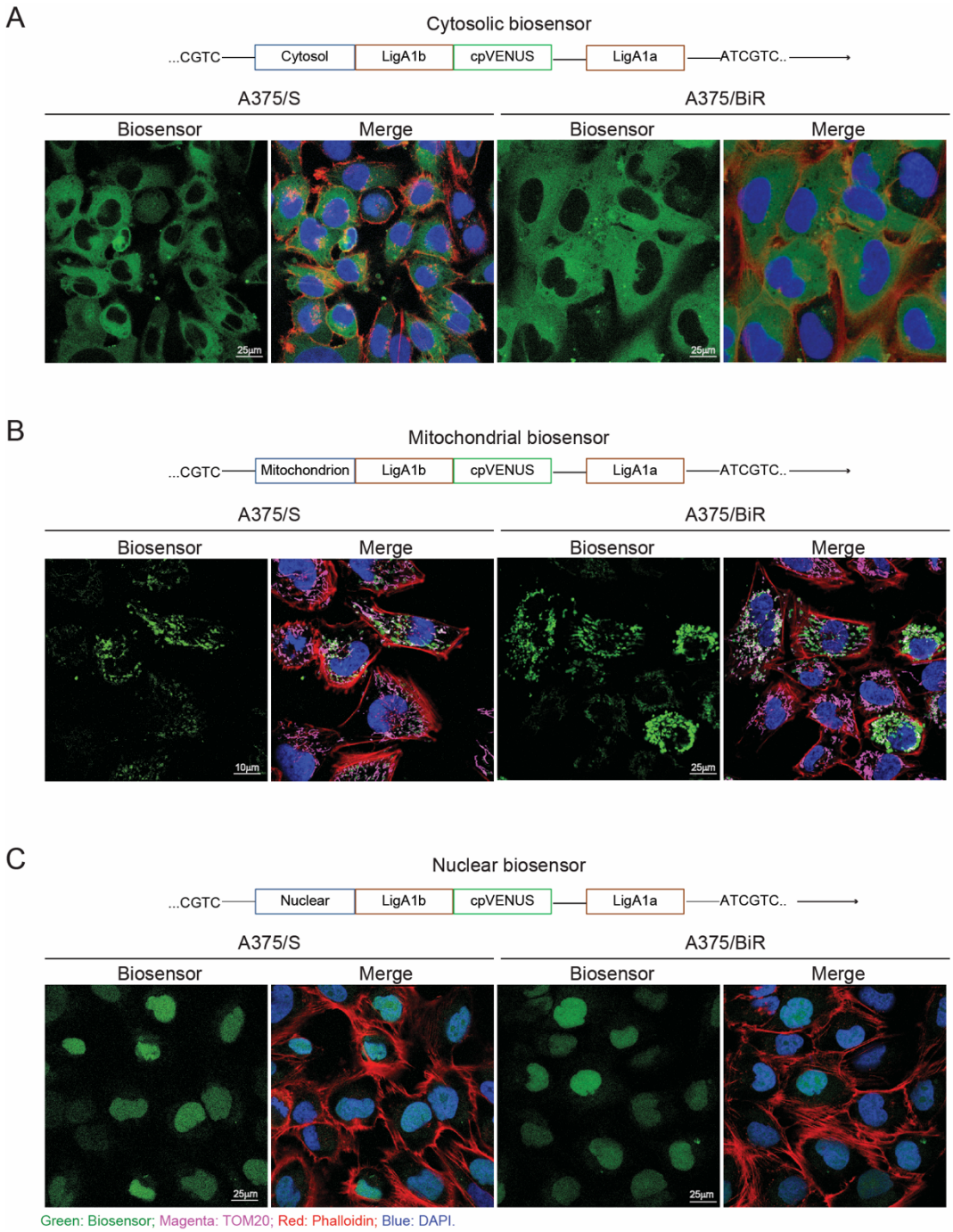

Figure 1. Generation of A375 cells stably expressing organelle-specific NAD$^+$ biosensors

(A,B,C) Confocal microscopy : cells were cultured on glass cover slips in 24-well plates, fixed (4% PFA), permeabilized (0.1% saponin) and saturated with pre-immune goat serum. Cells were counterstained with phalloidin (red), TOM20 (magenta) and DAPI (blue) to

highlight cytosol, mitochondria and nuclei, respectively. Fluorescence was acquired by confocal microscopy, using an oil immersion 63x objective. Slides were analyzed using a TCS SP5 laser scanning confocal microscope; images were acquired with LAS AF software Scale bar= 25µm for cytosolic A375 S/BiR, nuclear A375 S/BiR and mitochondrial A375/BiR; Scale bar= 10µm for mitochondrial A375/S. Diagrams on the top of each panel show the structure of the different constructs. A375/S **:** A375 sensitive to BRAF inhibitors; A375/BiR : A375 resistant to BRAF inhibitors.

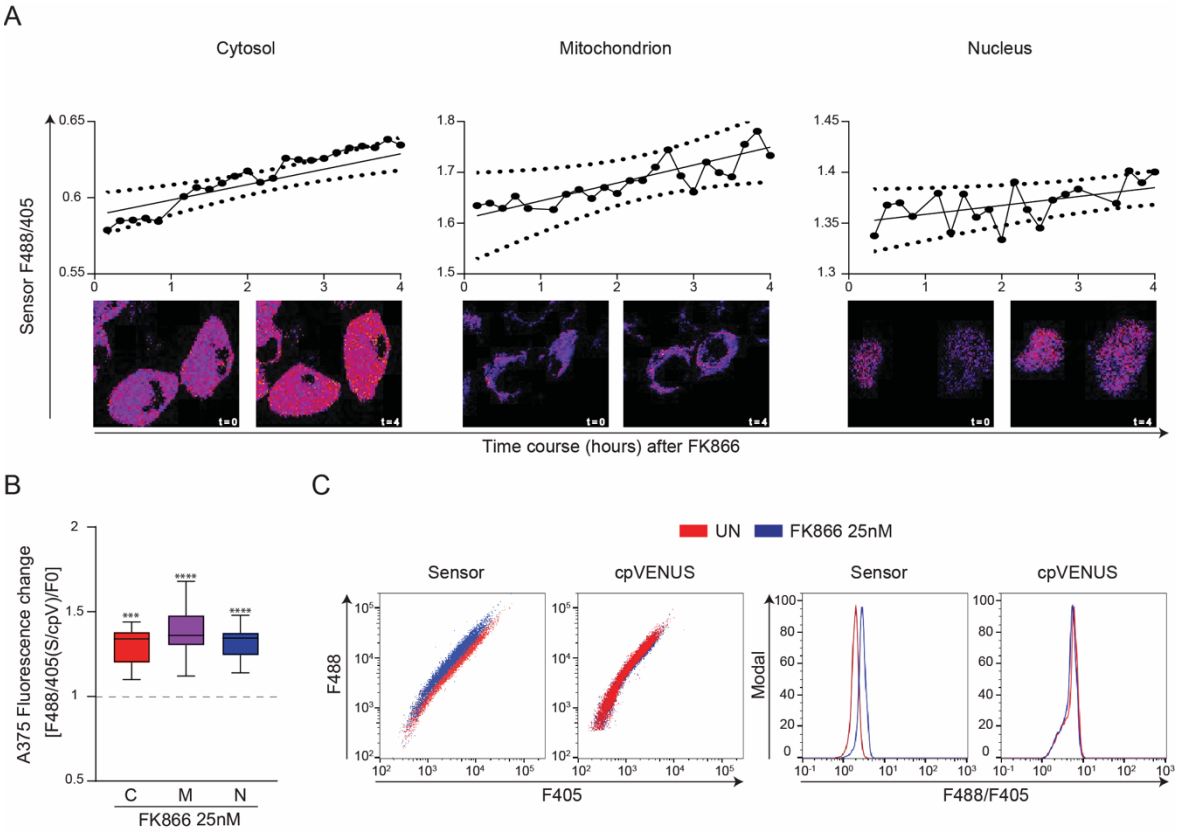

Figure 2. Effects of the NAMPT inhibitor FK866

(A) Upper: quantification of time lapse imaging of A375 cells expressing the cytosolic, mitochondrial and nuclear biosensor, in response to FK866 (25nM, 4h period). Cells were cultured on Ibidi chambered coverslips and kept at 5% CO_2 and 37°C during the experiment. Curves show the fluorescence ratio between 488 nm and 405 nm of the biosensor reported as a function of time. 488 nm and 405 nm fluorescence were separately recorded and the ratio was obtained by image calculator plugin of ImageJ software analysis. Curves are the results of 4 independent measurements. Lower: representative frames of A375 expressing relative biosensors at time (t) =0 and t=4. Fluorescence was acquired by confocal microscopy, using an oil immersion 63x objective, in the figure A cropped images from zoomed acquisition fields are shown. NAD^+ depletion can be followed by observing the increase of fluorescence intensity (movies 1-2-3)**.** (B) NAD^+ variations measured in A375 cytosol (C), mitochondria (M) and

nuclei (N) after treatment with FK866 (25 nM, 16 hours). Box plots are the results of 9 different experiments. Results are expressed as a "Ratio of Ratio" [F488/405(S/cpV)/F0]. Sensor/cpVenus (488 nm/405 nm) fluorescence ratios were measured by flow cytometry and the fold change compared with untreated controls (F0). (C) Representative example of fluorescence variation of the cytosolic biosensor upon FK866 treatment in A375. Dot plot (on the left) and histogram (on the right) show the specificity of the NAMPT inhibitor -induced NAD^+ depletion in increasing biosensor 488 nm fluorescence. UN: untreated.

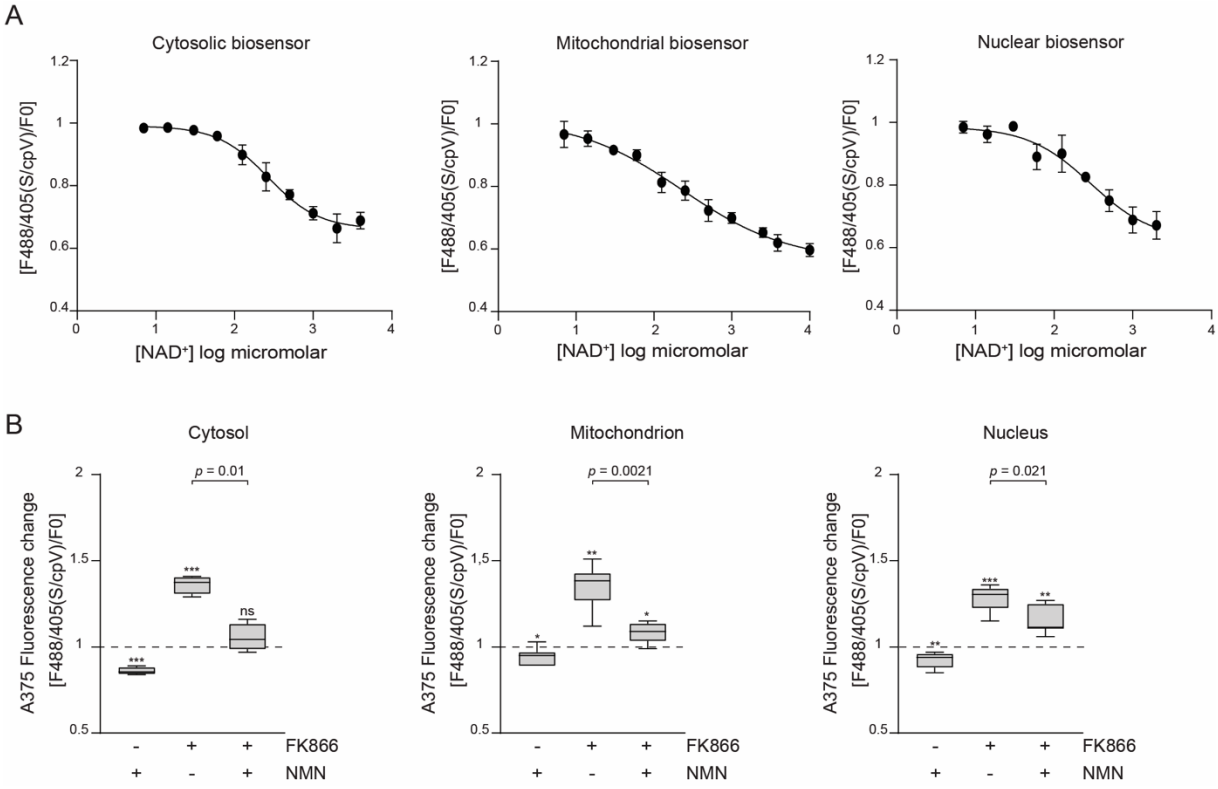

Figure 3. Subcellular NAD⁺ concentrations and effects of NMN on subcellular NAD⁺ levels

(A) Calibration curve of cytosolic, mitochondrial and nuclear biosensors obtained in A375. Cells were permeabilized with 0,005% saponin (cytosolic and nuclear biosensors) or with saponin and Alamethicin (mitochondrial biosensor expressing A375) and exposed to increased exogenous concentrations of NAD^+. The fluorescence ratios (488 nm/405 nm) of the biosensor were normalized to cpVENUS. Diagrams show normalized fluorescence ratios (*y*-axis) reported as a function of logarithmic NAD^+ concentrations (*x*-axis) and fit with a variable slope model. Curves are the results of 4 independent experiments.(B) Intracellular NAD^+ variations in A375 after treatment with NMN (0.5 mM, 16 hours), in presence or absence of FK866 25 nM (n=5). Results are expressed as a "Ratio of Ratio" [F488/405(S/coV)/F0]. Sensor/cpVenus (488 nm/405 nm) fluorescence

ratios were measured by flow cytometry and the fold change was compared to untreated controls (F0). Two-sided paired Student's t test was used to determine statistical significance. Star marks refer to the significance of the relative change of each treatments condition compared to the untreated (untreated=1), while the *p* value refers to the rescue of supplementations from the FK866-treated condition. Boxes represent interquartile range, and the horizontal line across each box indicates the median. ns= not statistically significant.

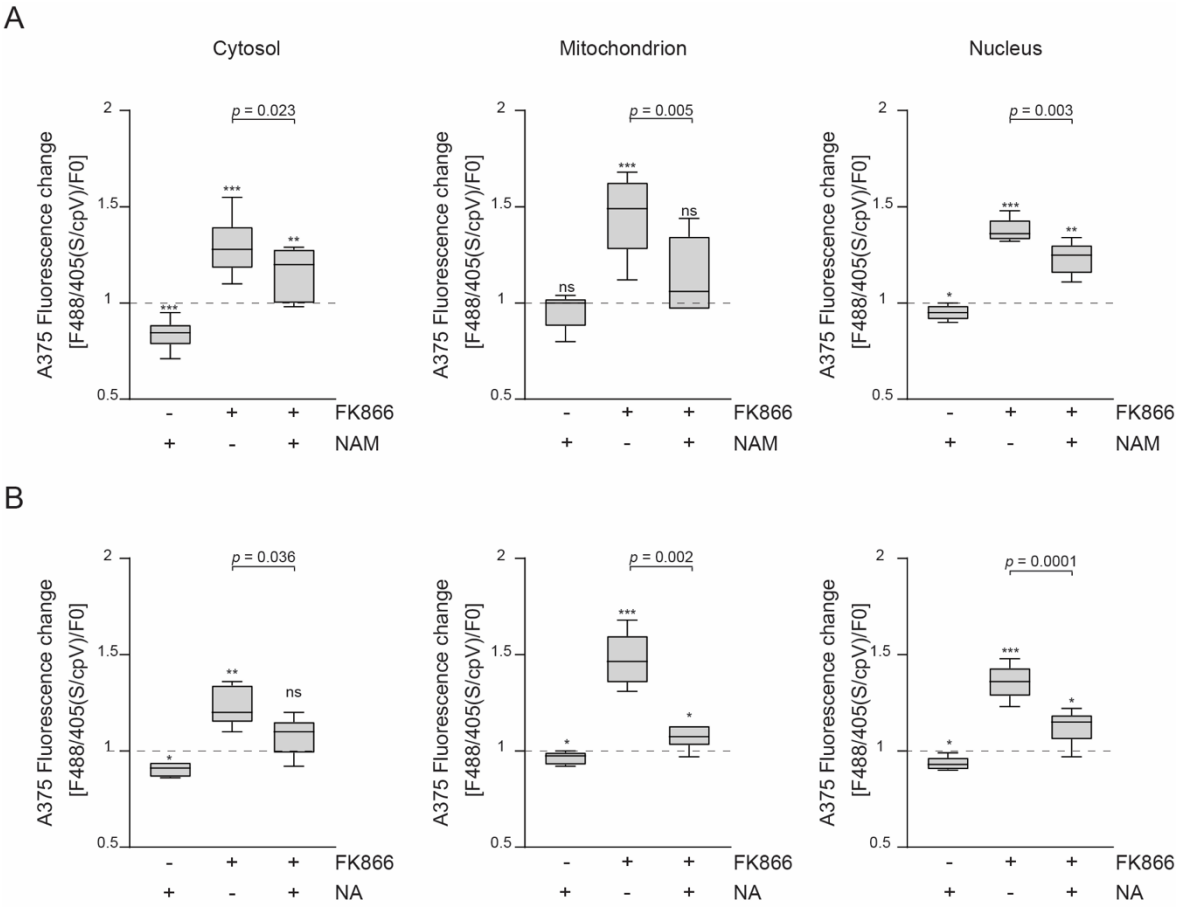

Figure 4. Topography of NAD⁺ Biosynthesis: NAM and NA primarily affect cytosolic NAD⁺ levels

Cells were treated as follows: (A) 500 µM NAM ± 25 nM FK866; (B) 6 µM NA ± 25 nM FK866. Results are expressed as a "Ratio of Ratio" [F488/405(S/coV)/F0]. Sensor/cpVenus (488 nm/405 nm) fluorescence ratios were measured by flow cytometry and the fold change was compared to untreated controls (F0) (n=5). Star marks refer to the significance of the relative change of each treatments condition compared to the untreated (untreated=1), while the *p* value refers to the rescue of supplementations from the FK866-treated condition.

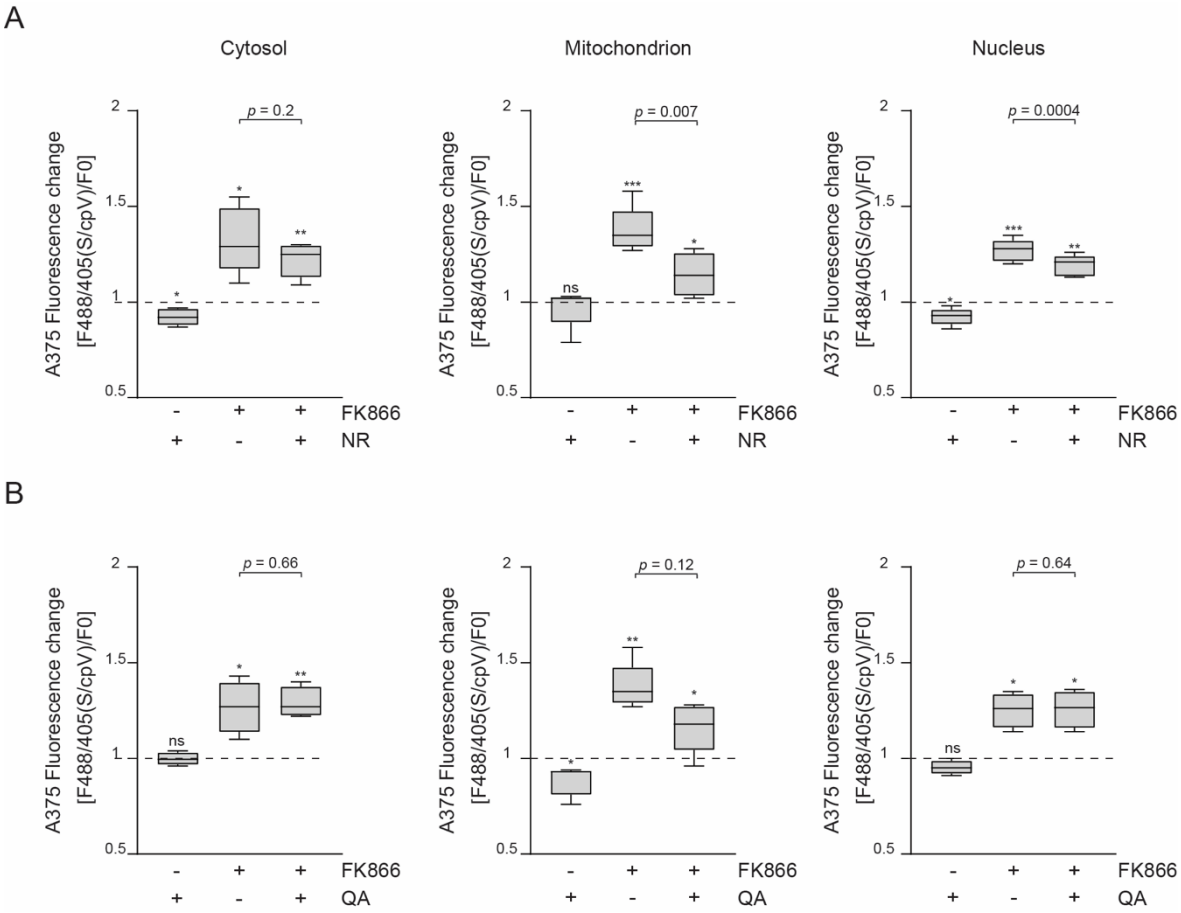

Figure 5. Topography of NAD⁺ Biosynthesis: NR and QA showed an organelle-specific impact on NAD⁺ levels

Cells were treated with (C) 100 µM NR ± 25 nM FK866; (D) 200 µM QA ± 25 nM FK866. A375 cells were exposed to the treatments for 16 hours. Results are expressed as a "Ratio of Ratio" [F488/405(S/coV)/F0]. Sensor/cpVenus (488 nm/405 nm) fluorescence ratios were measured by flow cytometry and the fold change was compared to untreated controls (F0) (n=5). Star marks refer to the significance of the relative change of each treatments condition compared to the untreated (untreated=1), while the *p* value refers to the rescue of supplementations from the FK866-treated condition.

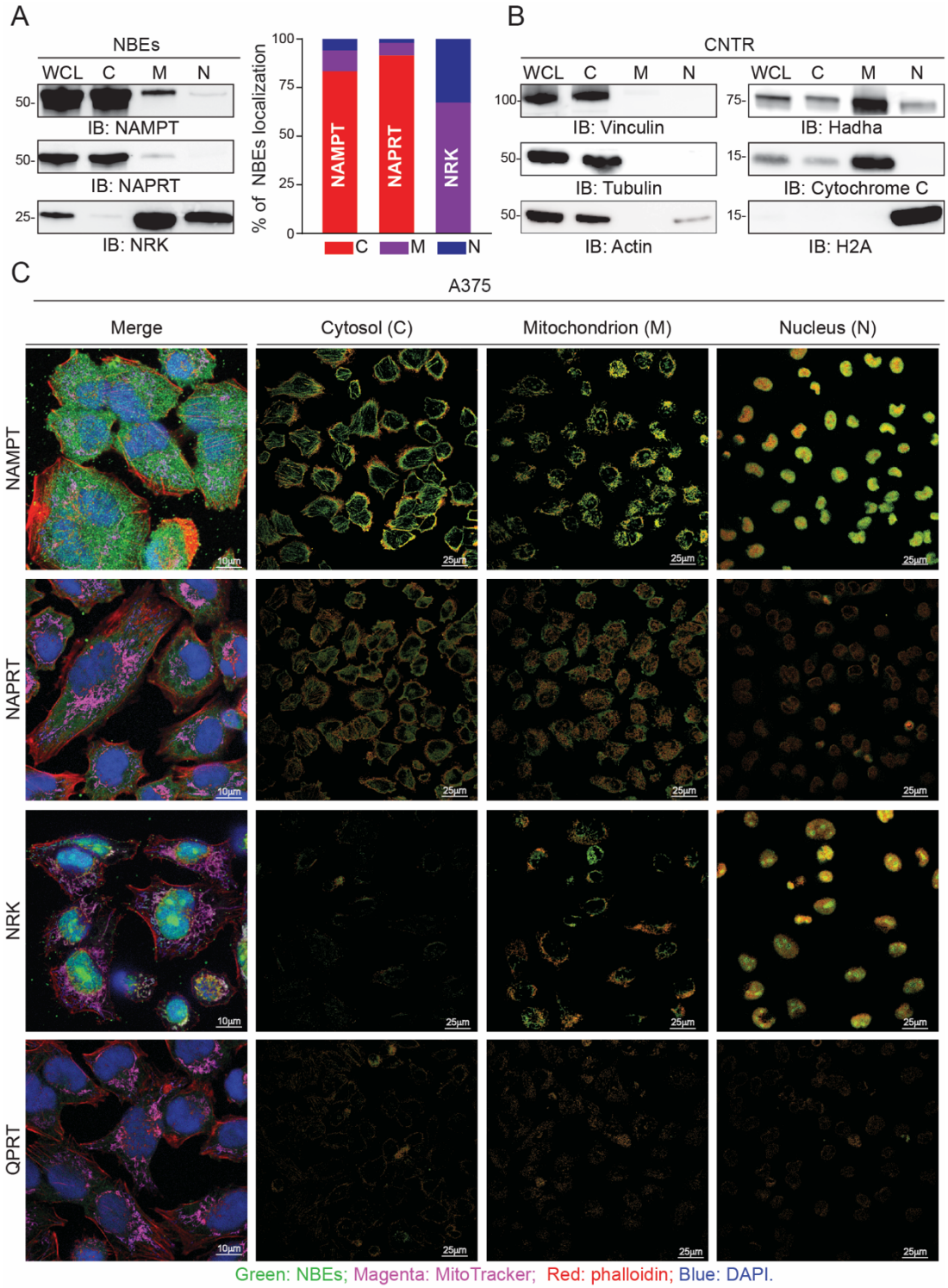

Figure 6. Subcellular localization of NAD⁺ biosynthetic enzymes

(A) Mitochondria and nuclei were isolated as described in material and methods. 10µg of each lysate were loaded in the following order: whole cell lysate (WCL), cytosolic fraction (C), mitochondrial fraction (M) and nuclear fraction (N). Anti-Vinculin, anti-

tubulin, anti-actin, anti-Hadha, anti-cytochrome c and anti-H2A were used to determine the purity of cytosolic, mitochondrial and nuclear fractions, respectively. (B) Graph represents the percentage of NBEs expression in each fraction. Band quantification was performed using ImageQuant software. Values are referred to the mean of 6 independent experiments. % was calculated as: % of pixel intensity of district specific band/sum of all districts pixel intensities. (C) On the left confocal microscopy showing NAMPT, NAPRT, NRK, QPRT total expression (green fluorescence) in whole cells (merge). Cytosol, mitochondria and nuclei were counterstained with phalloidin (red), MitoTracker (magenta) and DAPI (blue) respectively (zoomed image of 63X magnification, scale bar= 10µm). On the right NBEs-cytosol/mitochondria/nuclei sub-localization. In detail, NAMPT, NAPRT, NRK and QPRT (green fluorescence) were localized by delimiting fractions (red fluorescence) separately by using the co-localization tool of LAS AF Version Lite 2.4 software. Representative images show single NBE and single compartment overlapping (image of 63X magnification, scale bar= 25µm).

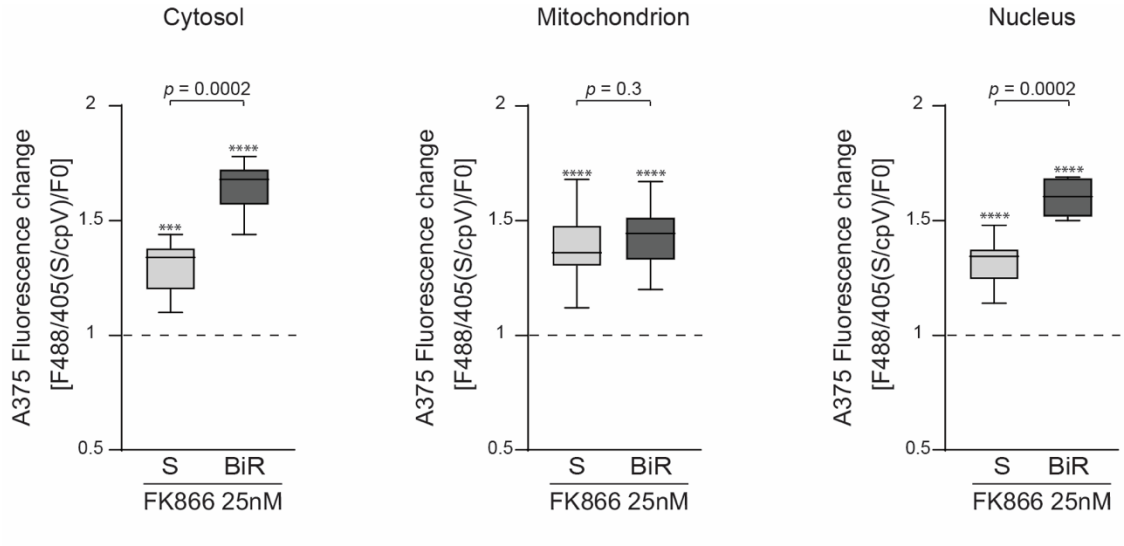

Figure 7. A375/S and /BiR responses to the NAMPT inhibition

Cytosolic, mitochondrial and nuclear NAD^+ variations were measured in BRAFi-sensitive (S) or resistant (BiR) cells after treatment with FK866 (25 nM, 16 hours). Results are expressed as relative fold change [F488/405(S/coV)/F0]. Sensor/cpVenus (488 nm/405 nm) fluorescence ratios were measured by flow cytometry and the fold change was compared to untreated (F0). Box plot representing 9 independent experiments. Star marks refers to the relative change of FK866 treatment compared to 1 (untreated), while p value indicates significance of the FK866 differential response of A375/BiR compared to A375/S.

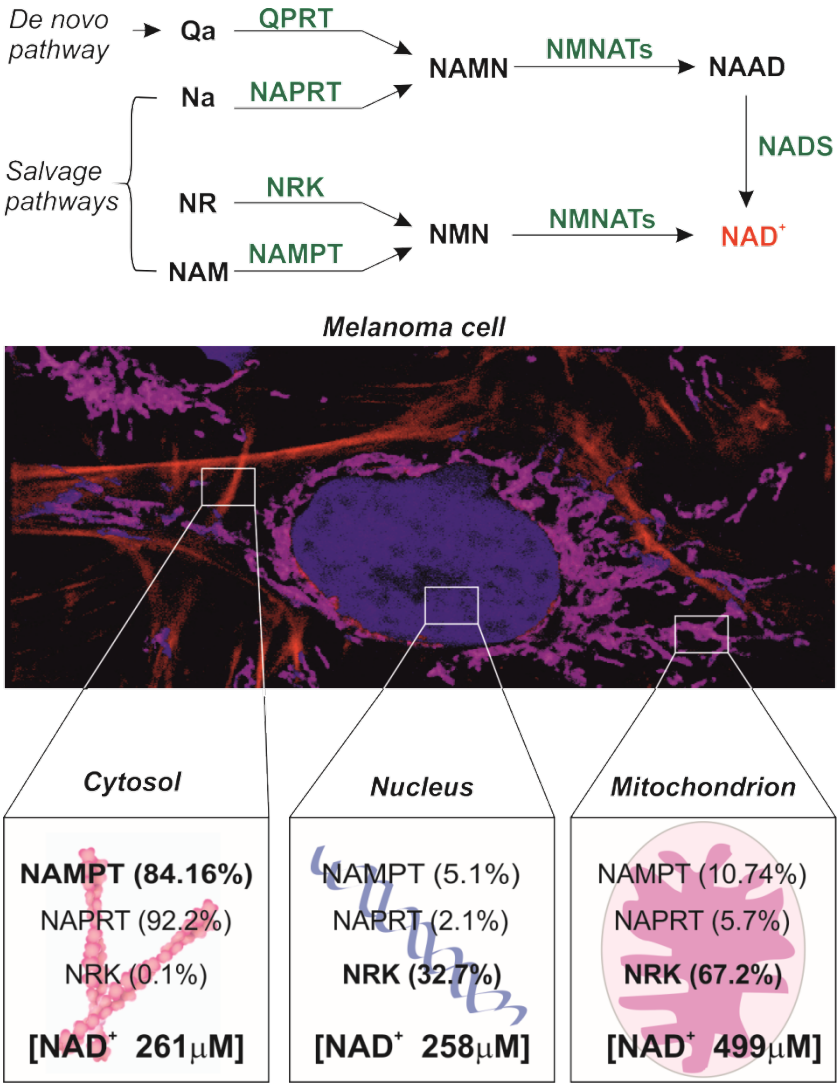

Figure 8. Compartmentalization of NAD⁺ biosynthesis in A375 MM

On the top schematic representation of biochemical reactions involved in NAD⁺ production. NAD⁺ precursors present in the extracellular space can enter the cell becoming substrates of the NBEs. QA enters in the *de novo* biosynthetic pathway, while NA, NR and NAM are substrates of the parallel three salvage pathways. Among the NAD⁺ precursors NAM is also the by-product of NAD⁺ consuming enzymes such as sirtuins and PARPs. NAM and NR can be used to produce NMN by NAMPT and NRKs, respectively. NMN and NaMN (produced by NAPRT-mediated Na conversion) are finally used by compartmentalized NMNATs to generate NAD⁺. In the center, an A375 melanoma cell acquired by using confocal microscope. Cytosol, mitochondria and nuclei were

counterstained with phalloidin (red), MitoTracker (magenta) and DAPI (blue) respectively (zoomed image of 63X magnification acquired by confocal microscopy , a cropped image is shown). Insets of A375 cytosol, nucleus and mitochondria resume the most relevant NBEs found in each A375 subcellular districts. Enzymes written in bold are the most expressed NBEs in the highlighted cell districts, while percentage refers to the expression level of each enzymes in each compartment. The cytosolic picture of A375 NAD^+ biosynthesis is composed by a dominant cytosolic NAMPT pathway converting NAM into NMN. NAPRT can be considered a second, but highly active, enzyme which mediates the cytosolic NA conversion to NaMN, indeed its localization was found to be more than 92% cytosolic. These pathways contribute to the generation of an NAD^+ pool calculated to be around 261 µM. In the nucleus, the NAD^+ pool is approximately 258 µM and the primary expressed NBEs is NRK. In this compartment, we were also able to detect low levels of NAMPT and NAPRT (5.1% and 2% of their total expression, respectively). NRK expression is also prevalent in mitochondria (67.2 % of its total biochemical detection), where the calculated NAD^+ concentration is 499 µM. In this organelle, low expression of NAMPT (10.74%) and NAPRT (5.7%) could contribute to the maintenance of mitochondrial NAD^+ pool.

[NAD^+ µM]	Cytoplasmic F488/F405 (S/cpV)	Mitochondrial F488/F405 (S/cpV)	Nuclear F488/F405 (S/cpV)
0	1	1	1
0.7	0.988	0.98	0.995
15	0.986	0.953	0.973
30	0.98	0.92	0.988
60	0.954	0.9	0.9
125	0.899	0.813	0.91
250	0.838	0.78	0.84
500	0.776	0.723	0.76
1000	0.71	0.7	0.712
2000	0.668	0.653	0.68
4000	0.66	0.62	N.D.
10000	N.D.	0.596	N.D.

Table 1. Fluorescence variations of each biosensors in the presence of NAD^+

Table showing cpVENUS normalized fluorescence variations of each biosensors when exposed to increasing concentrations of exogenous NAD^+ in a condition of saponin or saponin/alamethicin-mediated permeabilization. Reported numbers are the mean of four independent experiments for cytosolic and nuclear biosensor, of three independent experiments for mitochondrial biosensor.

References

1. Alano CC, Tran A, Tao R, Ying W, Karliner JS, Swanson RA. Differences among cell types in NAD(+) compartmentalization: a comparison of neurons, astrocytes, and cardiac myocytes. *J Neurosci Res* 85: 3378-85, 2007.
2. Allison SJ, Knight JR, Granchi C, Rani R, Minutolo F, Milner J, Phillips RM. Identification of LDH-A as a therapeutic target for cancer cell killing via (i) p53/NAD(H)-dependent and (ii) p53-independent pathways. *Oncogenesis* 3: e102, 2014.
3. Audrito V, Manago A, Gaudino F, Deaglio S. Targeting metabolic reprogramming in metastatic melanoma: The key role of nicotinamide phosphoribosyltransferase (NAMPT). *Semin Cell Dev Biol*, 2019.
4. Audrito V, Manago A, Gaudino F, Sorci L, Messana VG, Raffaelli N, Deaglio S. NAD-Biosynthetic and Consuming Enzymes as Central Players of Metabolic Regulation of Innate and Adaptive Immune Responses in Cancer. *Front Immunol* 10: 1720, 2019.
5. Audrito V, Manago A, La Vecchia S, Zamporlini F, Vitale N, Baroni G, Cignetto S, Serra S, Bologna C, Stingi A, Arruga F, Vaisitti T, Massi D, Mandala M, Raffaelli N, Deaglio S. Nicotinamide Phosphoribosyltransferase (NAMPT) as a Therapeutic Target in BRAF-Mutated Metastatic Melanoma. *J Natl Cancer Inst* 110, 2018.
6. Audrito V, Manago A, Zamporlini F, Rulli E, Gaudino F, Madonna G, D'Atri S, Antonini Cappellini GC, Ascierto PA, Massi D, Raffaelli N, Mandala M, Deaglio S. Extracellular nicotinamide phosphoribosyltransferase (eNAMPT) is a novel marker for patients with BRAF-mutated metastatic melanoma. *Oncotarget* 9: 18997-19005, 2018.
7. Batandier C, Leverve X, Fontaine E. Opening of the mitochondrial permeability transition pore induces reactive oxygen species production at the level of the respiratory chain complex I. *J Biol Chem* 279: 17197-204, 2004.

8. Belenky P, Christensen KC, Gazzaniga F, Pletnev AA, Brenner C. Nicotinamide riboside and nicotinic acid riboside salvage in fungi and mammals. Quantitative basis for Urh1 and purine nucleoside phosphorylase function in NAD+ metabolism. *J Biol Chem* 284: 158-64, 2009.

9. Bender DA. Biochemistry of tryptophan in health and disease. *Mol Aspects Med* 6: 101-97, 1983.

10. Berger F, Lau C, Dahlmann M, Ziegler M. Subcellular compartmentation and differential catalytic properties of the three human nicotinamide mononucleotide adenylyltransferase isoforms. *J Biol Chem* 280: 36334-41, 2005.

11. Berger F, Ramirez-Hernandez MH, Ziegler M. The new life of a centenarian: signalling functions of NAD(P). *Trends Biochem Sci* 29: 111-8, 2004.

12. Bilan DS, Matlashov ME, Gorokhovatsky AY, Schultz C, Enikolopov G, Belousov VV. Genetically encoded fluorescent indicator for imaging NAD(+)/NADH ratio changes in different cellular compartments. *Biochim Biophys Acta* 1840: 951-7, 2014.

13. Bitterman KJ, Anderson RM, Cohen HY, Latorre-Esteves M, Sinclair DA. Inhibition of silencing and accelerated aging by nicotinamide, a putative negative regulator of yeast sir2 and human SIRT1. *J Biol Chem* 277: 45099-107, 2002.

14. Bomar L, Senithilnathan A, Ahn C. Systemic Therapies for Advanced Melanoma. *Dermatol Clin* 37: 409-423, 2019.

15. Brun MA, Tan KT, Nakata E, Hinner MJ, Johnsson K. Semisynthetic fluorescent sensor proteins based on self-labeling protein tags. *J Am Chem Soc* 131: 5873-84, 2009.

16. Cairns RA, Harris IS, Mak TW. Regulation of cancer cell metabolism. *Nat Rev Cancer* 11: 85-95, 2011.

17. Cambronne XA, Stewart ML, Kim D, Jones-Brunette AM, Morgan RK, Farrens DL, Cohen MS, Goodman RH. Biosensor reveals multiple sources for mitochondrial NAD(+). *Science* 352: 1474-7, 2016.

18. Cameron WD, Bui CV, Hutchinson A, Loppnau P, Graslund S, Rocheleau JV. Apollo-NADP(+): a spectrally tunable family of genetically encoded sensors for NADP(+). *Nat Methods* 13: 352-8, 2016.

19. Canto C, Menzies KJ, Auwerx J. NAD(+) Metabolism and the Control of Energy Homeostasis: A Balancing Act between Mitochondria and the Nucleus. *Cell Metab* 22: 31-53, 2015.

20. Cerna D, Li H, Flaherty S, Takebe N, Coleman CN, Yoo SS. Inhibition of nicotinamide phosphoribosyltransferase (NAMPT) activity by small molecule GMX1778 regulates reactive oxygen species (ROS)-mediated cytotoxicity in a p53- and nicotinic acid phosphoribosyltransferase1 (NAPRT1)-dependent manner. *J Biol Chem* 287: 22408-17, 2012.

21. Chen H, Wang S, Zhang H, Nice EC, Huang C. Nicotinamide phosphoribosyltransferase (Nampt) in carcinogenesis: new clinical opportunities. *Expert Rev Anticancer Ther* 16: 827-38, 2016.

22. Chiarugi A, Dolle C, Felici R, Ziegler M. The NAD metabolome--a key determinant of cancer cell biology. *Nat Rev Cancer* 12: 741-52, 2012.

23. Chio IIC, Tuveson DA. ROS in Cancer: The Burning Question. *Trends Mol Med* 23: 411-429, 2017.

24. Chowdhry S, Zanca C, Rajkumar U, Koga T, Diao Y, Raviram R, Liu F, Turner K, Yang H, Brunk E, Bi J, Furnari F, Bafna V, Ren B, Mischel PS. NAD metabolic dependency in cancer is shaped by gene amplification and enhancer remodelling. *Nature* 569: 570-575, 2019.

25. Cohen MS, Stewart ML, Goodman RH, Cambronne XA. Methods for Using a Genetically Encoded Fluorescent Biosensor to Monitor Nuclear NAD<sup/>. *Methods Mol Biol* 1813: 391-414, 2018.

26. Connell NJ, Houtkooper RH, Schrauwen P. NAD(+) metabolism as a target for metabolic health: have we found the silver bullet? *Diabetologia*, 2019.

27. Davila A, Liu L, Chellappa K, Redpath P, Nakamaru-Ogiso E, Paolella LM, Zhang Z, Migaud ME, Rabinowitz JD, Baur JA. Nicotinamide adenine dinucleotide is transported into mammalian mitochondria. *Elife* 7, 2018.

28. Di Stefano M, Conforti L. Diversification of NAD biological role: the importance of location. *FEBS J* 280: 4711-28, 2013.

29. Eggermont AM. Adjuvant ipilimumab in stage III melanoma: New landscape, new questions. *Eur J Cancer* 69: 39-42, 2016.

30. Eller JM, Stewart ML, Slepian AJ, Markwardt S, Wiedrick J, Cohen MS, Goodman RH, Cambronne XA. Flow Cytometry Analysis of Free Intracellular NAD(+) Using a Targeted Biosensor. *Curr Protoc Cytom* 88: e54, 2019.

31. Fan J, Ye J, Kamphorst JJ, Shlomi T, Thompson CB, Rabinowitz JD. Quantitative flux analysis reveals folate-dependent NADPH production. *Nature* 510: 298-302, 2014.

32. Felici R, Lapucci A, Ramazzotti M, Chiarugi A. Insight into molecular and functional properties of NMNAT3 reveals new hints of NAD homeostasis within human mitochondria. *PLoS One* 8: e76938, 2013.

33. Fischer E, Zamboni N, Sauer U. High-throughput metabolic flux analysis based on gas chromatography-mass spectrometry derived 13C constraints. *Anal Biochem* 325: 308-16, 2004.

34. Flaherty KT, Infante JR, Daud A, Gonzalez R, Kefford RF, Sosman J, Hamid O, Schuchter L, Cebon J, Ibrahim N, Kudchadkar R, Burris HA, 3rd, Falchook G, Algazi A, Lewis K, Long GV, Puzanov I, Lebowitz P, Singh A, Little S, Sun P, Allred A, Ouellet D, Kim KB, Patel K, Weber J. Combined BRAF and MEK inhibition in melanoma with BRAF V600 mutations. *N Engl J Med* 367: 1694-703, 2012.

35. Fons NR, Sundaram RK, Breuer GA, Peng S, McLean RL, Kalathil AN, Schmidt MS, Carvalho DM, Mackay A, Jones C, Carcaboso AM, Nazarian J, Berens ME, Brenner C, Bindra RS. PPM1D

mutations silence NAPRT gene expression and confer NAMPT inhibitor sensitivity in glioma. *Nat Commun* 10: 3790, 2019.

36. Frezza C, Cipolat S, Scorrano L. Organelle isolation: functional mitochondria from mouse liver, muscle and cultured fibroblasts. *Nat Protoc* 2: 287-95, 2007.

37. Garten A, Schuster S, Penke M, Gorski T, de Giorgis T, Kiess W. Physiological and pathophysiological roles of NAMPT and NAD metabolism. *Nat Rev Endocrinol* 11: 535-46, 2015.

38. Gostimskaya IS, Grivennikova VG, Zharova TV, Bakeeva LE, Vinogradov AD. In situ assay of the intramitochondrial enzymes: use of alamethicin for permeabilization of mitochondria. *Anal Biochem* 313: 46-52, 2003.

39. Grahnert A, Grahnert A, Klein C, Schilling E, Wehrhahn J, Hauschildt S. Review: NAD +: a modulator of immune functions. *Innate Immun* 17: 212-33, 2011.

40. Green RM, Graham M, O'Donovan MR, Chipman JK, Hodges NJ. Subcellular compartmentalization of glutathione: correlations with parameters of oxidative stress related to genotoxicity. *Mutagenesis* 21: 383-90, 2006.

41. Grozio A, Sociali G, Sturla L, Caffa I, Soncini D, Salis A, Raffaelli N, De Flora A, Nencioni A, Bruzzone S. CD73 protein as a source of extracellular precursors for sustained NAD+ biosynthesis in FK866-treated tumor cells. *J Biol Chem* 288: 25938-49, 2013.

42. Gujar AD, Le S, Mao DD, Dadey DY, Turski A, Sasaki Y, Aum D, Luo J, Dahiya S, Yuan L, Rich KM, Milbrandt J, Hallahan DE, Yano H, Tran DD, Kim AH. An NAD+-dependent transcriptional program governs self-renewal and radiation resistance in glioblastoma. *Proc Natl Acad Sci U S A* 113: E8247-E8256, 2016.

43. Hasmann M, Schemainda I. FK866, a highly specific noncompetitive inhibitor of nicotinamide phosphoribosyltransferase, represents a novel mechanism for induction of tumor cell apoptosis. *Cancer Res* 63: 7436-42, 2003.

44. Hassinen IE. Signaling and Regulation Through the NAD(+) and NADP(+) Networks. *Antioxid Redox Signal* 30: 857-874, 2019.

45. Holen K, Saltz LB, Hollywood E, Burk K, Hanauske AR. The pharmacokinetics, toxicities, and biologic effects of FK866, a nicotinamide adenine dinucleotide biosynthesis inhibitor. *Invest New Drugs* 26: 45-51, 2008.

46. Hou J, Chong ZZ, Shang YC, Maiese K. Early apoptotic vascular signaling is determined by Sirt1 through nuclear shuttling, forkhead trafficking, bad, and mitochondrial caspase activation. *Curr Neurovasc Res* 7: 95-112, 2010.

47. Houtkooper RH, Canto C, Wanders RJ, Auwerx J. The secret life of NAD+: an old metabolite controlling new metabolic signaling pathways. *Endocr Rev* 31: 194-223, 2010.

48. Hu-Lieskovan S, Mok S, Homet Moreno B, Tsoi J, Robert L, Goedert L, Pinheiro EM, Koya RC, Graeber TG, Comin-Anduix B, Ribas A. Improved antitumor activity of immunotherapy with BRAF and MEK inhibitors in BRAF(V600E) melanoma. *Sci Transl Med* 7: 279ra41, 2015.

49. Hung YP, Albeck JG, Tantama M, Yellen G. Imaging cytosolic NADH-NAD(+) redox state with a genetically encoded fluorescent biosensor. *Cell Metab* 14: 545-54, 2011.

50. Imai S, Guarente L. NAD+ and sirtuins in aging and disease. *Trends Cell Biol* 24: 464-71, 2014.

51. Karpov AS, Abrams T, Clark S, Raikar A, D'Alessio JA, Dillon MP, Gesner TG, Jones D, Lacaud M, Mallet W, Martyniuk P, Meredith E, Mohseni M, Nieto-Oberhuber CM, Palacios D, Perruccio F, Piizzi G, Zurini M, Bialucha CU. Nicotinamide Phosphoribosyltransferase Inhibitor as a Novel Payload for Antibody-Drug Conjugates. *ACS Med Chem Lett* 9: 838-842, 2018.

52. Kennedy BE, Sharif T, Martell E, Dai C, Kim Y, Lee PW, Gujar SA. NAD(+) salvage pathway in cancer metabolism and therapy. *Pharmacol Res* 114: 274-283, 2016.

53. Keppler A, Gendreizig S, Gronemeyer T, Pick H, Vogel H, Johnsson K. A general method for the covalent labeling of fusion proteins with small molecules in vivo. *Nat Biotechnol* 21: 86-9, 2003.

54. Koch-Nolte F, Fischer S, Haag F, Ziegler M. Compartmentation of NAD+-dependent signalling. *FEBS Lett* 585: 1651-6, 2011.

55. Kulkarni CA, Brookes P. Cellular Compartmentation and the Redox/Non-Redox Functions of NAD⁺. *Antioxid Redox Signal*, 2019.

56. Kusumanchi P, Zhang Y, Jani MB, Jayaram NH, Khan RA, Tang Y, Antony AC, Jayaram HN. Nicotinamide mononucleotide adenylyltransferase2 overexpression enhances colorectal cancer cell-kill by Tiazofurin. *Cancer Gene Ther* 20: 403-12, 2013.

57. Leanza L, Henry B, Sassi N, Zoratti M, Chandy KG, Gulbins E, Szabo I. Inhibitors of mitochondrial Kv1.3 channels induce Bax/Bak-independent death of cancer cells. *EMBO Mol Med* 4: 577-93, 2012.

58. Li XQ, Lei J, Mao LH, Wang QL, Xu F, Ran T, Zhou ZH, He S. NAMPT and NAPRT, Key Enzymes in NAD Salvage Synthesis Pathway, Are of Negative Prognostic Value in Colorectal Cancer. *Front Oncol* 9: 736, 2019.

59. Liou GY, Storz P. Reactive oxygen species in cancer. *Free Radic Res* 44: 479-96, 2010.

60. Los GV, Encell LP, McDougall MG, Hartzell DD, Karassina N, Zimprich C, Wood MG, Learish R, Ohana RF, Urh M, Simpson D, Mendez J, Zimmerman K, Otto P, Vidugiris G, Zhu J, Darzins A, Klaubert DH, Bulleit RF, Wood KV. HaloTag: a novel protein labeling technology for cell imaging and protein analysis. *ACS Chem Biol* 3: 373-82, 2008.

61. Lowry OH, Passonneau JV, Schulz DW, Rock MK. The measurement of pyridine nucleotides by enzymatic cycling. *J Biol Chem* 236: 2746-55, 1961.

62. Magni G, Amici A, Emanuelli M, Orsomando G, Raffaelli N, Ruggieri S. Enzymology of NAD+ homeostasis in man. *Cell Mol Life Sci* 61: 19-34, 2004.

63. Maldi E, Travelli C, Caldarelli A, Agazzone N, Cintura S, Galli U, Scatolini M, Ostano P, Miglino B, Chiorino G, Boldorini R, Genazzani AA. Nicotinamide phosphoribosyltransferase (NAMPT) is over-expressed in melanoma lesions. *Pigment Cell Melanoma Res* 26: 144-6, 2013.

64. Martens CR, Denman BA, Mazzo MR, Armstrong ML, Reisdorph N, McQueen MB, Chonchol M, Seals DR. Chronic nicotinamide riboside supplementation is well-tolerated and elevates NAD(+) in healthy middle-aged and older adults. *Nat Commun* 9: 1286, 2018.

65. Matic S, Geisler DA, Moller IM, Widell S, Rasmusson AG. Alamethicin permeabilizes the plasma membrane and mitochondria but not the tonoplast in tobacco (Nicotiana tabacum L. cv Bright Yellow) suspension cells. *Biochem J* 389: 695-704, 2005.

66. Montecucco F, Bauer I, Braunersreuther V, Bruzzone S, Akhmedov A, Luscher TF, Speer T, Poggi A, Mannino E, Pelli G, Galan K, Bertolotto M, Lenglet S, Garuti A, Montessuit C, Lerch R, Pellieux C, Vuilleumier N, Dallegri F, Mage J, Sebastian C, Mostoslavsky R, Gayet-Ageron A, Patrone F, Mach F, Nencioni A. Inhibition of nicotinamide phosphoribosyltransferase reduces neutrophil-mediated injury in myocardial infarction. *Antioxid Redox Signal* 18: 630-41, 2013.

67. Montecucco F, Cea M, Bauer I, Soncini D, Caffa I, Lasiglie D, Nahimana A, Uccelli A, Bruzzone S, Nencioni A. Nicotinamide phosphoribosyltransferase (NAMPT) inhibitors as therapeutics: rationales, controversies, clinical experience. *Curr Drug Targets* 14: 637-43, 2013.

68. Morgan B, Ezerina D, Amoako TN, Riemer J, Seedorf M, Dick TP. Multiple glutathione disulfide removal pathways mediate cytosolic redox homeostasis. *Nat Chem Biol* 9: 119-25, 2013.

69. Nikiforov A, Dolle C, Niere M, Ziegler M. Pathways and subcellular compartmentation of NAD biosynthesis in human cells: from entry of extracellular precursors to mitochondrial NAD generation. *J Biol Chem* 286: 21767-78, 2011.

70. Nobrega-Pereira S, Fernandez-Marcos PJ, Brioche T, Gomez-Cabrera MC, Salvador-Pascual A, Flores JM, Vina J, Serrano M. G6PD protects from oxidative damage and improves healthspan in mice. *Nat Commun* 7: 10894, 2016.

71. O'Callaghan C, Vassilopoulos A. Sirtuins at the crossroads of stemness, aging, and cancer. *Aging Cell* 16: 1208-1218, 2017.

72. Palmieri F, Rieder B, Ventrella A, Blanco E, Do PT, Nunes-Nesi A, Trauth AU, Fiermonte G, Tjaden J, Agrimi G, Kirchberger S, Paradies E, Fernie AR, Neuhaus HE. Molecular identification and functional characterization of Arabidopsis thaliana mitochondrial and chloroplastic NAD+ carrier proteins. *J Biol Chem* 284: 31249-59, 2009.

73. Parmenter TJ, Kleinschmidt M, Kinross KM, Bond ST, Li J, Kaadige MR, Rao A, Sheppard KE, Hugo W, Pupo GM, Pearson RB, McGee SL, Long GV, Scolyer RA, Rizos H, Lo RS, Cullinane C, Ayer DE, Ribas A, Johnstone RW, Hicks RJ, McArthur GA. Response of BRAF-mutant melanoma to BRAF inhibition is mediated by a network of transcriptional regulators of glycolysis. *Cancer Discov* 4: 423-33, 2014.

74. Piacente F, Caffa I, Ravera S, Sociali G, Passalacqua M, Vellone VG, Becherini P, Reverberi D, Monacelli F, Ballestrero A, Odetti P, Cagnetta A, Cea M, Nahimana A, Duchosal M, Bruzzone S, Nencioni A. Nicotinic Acid Phosphoribosyltransferase Regulates Cancer Cell Metabolism, Susceptibility to NAMPT Inhibitors, and DNA Repair. *Cancer Res* 77: 3857-3869, 2017.

75. Pirinen E, Canto C, Jo YS, Morato L, Zhang H, Menzies KJ, Williams EG, Mouchiroud L, Moullan N, Hagberg C, Li W, Timmers S, Imhof R, Verbeek J, Pujol A, van Loon B, Viscomi C, Zeviani M, Schrauwen P, Sauve AA, Schoonjans K, Auwerx J. Pharmacological Inhibition of poly(ADP-ribose) polymerases improves fitness and mitochondrial function in skeletal muscle. *Cell Metab* 19: 1034-41, 2014.

76. Pittelli M, Felici R, Pitozzi V, Giovannelli L, Bigagli E, Cialdai F, Romano G, Moroni F, Chiarugi A. Pharmacological effects of exogenous NAD on mitochondrial bioenergetics, DNA repair, and apoptosis. *Mol Pharmacol* 80: 1136-46, 2011.

77. Queirolo P, Dozin B, Morabito A, Banelli B, Piccioli P, Fava C, Leo C, Carosio R, Laurent S, Fontana V, Ferrucci PF, Martinoli C, Cocorocchio E, Battaglia A, Ascierto PA, Capone M, Simeone E, De Galitiis F, Pagani E, Antonini Cappellini GC, Marchetti P, Guida M, Tommasi S, Mandala M, Merelli B, Quaglino P, Fava P, Guidoboni M, Romani M, Spagnolo F, Pistillo MP. Corrigendum: Association of CTLA-4 Gene Variants with Response to Therapy and Long-term

Survival in Metastatic Melanoma Patients Treated with Ipilimumab: An Italian Melanoma Intergroup Study. *Front Immunol* 9: 403, 2018.

78. Raffaelli N, Sorci L, Amici A, Emanuelli M, Mazzola F, Magni G. Identification of a novel human nicotinamide mononucleotide adenylyltransferase. *Biochem Biophys Res Commun* 297: 835-40, 2002.

79. Rajman L, Chwalek K, Sinclair DA. Therapeutic Potential of NAD-Boosting Molecules: The In Vivo Evidence. *Cell Metab* 27: 529-547, 2018.

80. Ratajczak J, Joffraud M, Trammell SA, Ras R, Canela N, Boutant M, Kulkarni SS, Rodrigues M, Redpath P, Migaud ME, Auwerx J, Yanes O, Brenner C, Canto C. NRK1 controls nicotinamide mononucleotide and nicotinamide riboside metabolism in mammalian cells. *Nat Commun* 7: 13103, 2016.

81. Revollo JR, Grimm AA, Imai S. The NAD biosynthesis pathway mediated by nicotinamide phosphoribosyltransferase regulates Sir2 activity in mammalian cells. *J Biol Chem* 279: 50754-63, 2004.

82. Revollo JR, Grimm AA, Imai S. The regulation of nicotinamide adenine dinucleotide biosynthesis by Nampt/PBEF/visfatin in mammals. *Curr Opin Gastroenterol* 23: 164-70, 2007.

83. Revollo JR, Korner A, Mills KF, Satoh A, Wang T, Garten A, Dasgupta B, Sasaki Y, Wolberger C, Townsend RR, Milbrandt J, Kiess W, Imai S. Nampt/PBEF/Visfatin regulates insulin secretion in beta cells as a systemic NAD biosynthetic enzyme. *Cell Metab* 6: 363-75, 2007.

84. Rongvaux A, Andris F, Van Gool F, Leo O. Reconstructing eukaryotic NAD metabolism. *Bioessays* 25: 683-90, 2003.

85. Sallin O, Reymond L, Gondrand C, Raith F, Koch B, Johnsson K. Semisynthetic biosensors for mapping cellular concentrations of nicotinamide adenine dinucleotides. *Elife* 7, 2018.

86. Sauve AA, Wolberger C, Schramm VL, Boeke JD. The biochemistry of sirtuins. *Annu Rev Biochem* 75: 435-65, 2006.

87. Schulze A, Harris AL. How cancer metabolism is tuned for proliferation and vulnerable to disruption. *Nature* 491: 364-73, 2012.

88. Shackelford RE, Mayhall K, Maxwell NM, Kandil E, Coppola D. Nicotinamide phosphoribosyltransferase in malignancy: a review. *Genes Cancer* 4: 447-56, 2013.

89. Shain AH, Bastian BC. From melanocytes to melanomas. *Nat Rev Cancer* 16: 345-58, 2016.

90. Sharif T, Martell E, Dai C, Ghassemi-Rad MS, Kennedy BE, Lee PWK, Gujar S. Regulation of Cancer and Cancer-Related Genes via NAD(). *Antioxid Redox Signal*, 2018.

91. Soncini D, Caffa I, Zoppoli G, Cea M, Cagnetta A, Passalacqua M, Mastracci L, Boero S, Montecucco F, Sociali G, Lasiglie D, Damonte P, Grozio A, Mannino E, Poggi A, D'Agostino VG, Monacelli F, Provenzani A, Odetti P, Ballestrero A, Bruzzone S, Nencioni A. Nicotinamide phosphoribosyltransferase promotes epithelial-to-mesenchymal transition as a soluble factor independent of its enzymatic activity. *J Biol Chem* 289: 34189-204, 2014.

92. Stein LR, Imai S. The dynamic regulation of NAD metabolism in mitochondria. *Trends Endocrinol Metab* 23: 420-8, 2012.

93. Tarrado-Castellarnau M, de Atauri P, Cascante M. Oncogenic regulation of tumor metabolic reprogramming. *Oncotarget* 7: 62726-62753, 2016.

94. Todisco S, Agrimi G, Castegna A, Palmieri F. Identification of the mitochondrial NAD+ transporter in Saccharomyces cerevisiae. *J Biol Chem* 281: 1524-31, 2006.

95. Topalian SL, Drake CG, Pardoll DM. Targeting the PD-1/B7-H1(PD-L1) pathway to activate anti-tumor immunity. *Curr Opin Immunol* 24: 207-12, 2012.

96. Trammell SA, Schmidt MS, Weidemann BJ, Redpath P, Jaksch F, Dellinger RW, Li Z, Abel ED, Migaud ME, Brenner C. Nicotinamide riboside is uniquely and orally bioavailable in mice and humans. *Nat Commun* 7: 12948, 2016.

97. Travelli C, Aprile S, Mattoteia D, Colombo G, Clemente N, Scanziani E, Terrazzino S, Alisi MA, Polenzani L, Grosa G, Genazzani AA, Tron GC, Galli U. Identification of potent triazolylpyridine

nicotinamide phosphoribosyltransferase (NAMPT) inhibitors bearing a 1,2,3-triazole tail group. *Eur J Med Chem* 181: 111576, 2019.

98. Verdin E. NAD(+) in aging, metabolism, and neurodegeneration. *Science* 350: 1208-13, 2015.

99. von Heideman A, Berglund A, Larsson R, Nygren P. Safety and efficacy of NAD depleting cancer drugs: results of a phase I clinical trial of CHS 828 and overview of published data. *Cancer Chemother Pharmacol* 65: 1165-72, 2010.

100. Xiao W, Wang RS, Handy DE, Loscalzo J. NAD(H) and NADP(H) Redox Couples and Cellular Energy Metabolism. *Antioxid Redox Signal* 28: 251-272, 2018.

101. Xie W, Xu A, Yeung ES. Determination of NAD(+) and NADH in a single cell under hydrogen peroxide stress by capillary electrophoresis. *Anal Chem* 81: 1280-4, 2009.

102. Xu TY, Zhang SL, Dong GQ, Liu XZ, Wang X, Lv XQ, Qian QJ, Zhang RY, Sheng CQ, Miao CY. Discovery and characterization of novel small-molecule inhibitors targeting nicotinamide phosphoribosyltransferase. *Sci Rep* 5: 10043, 2015.

103. Yaku K, Okabe K, Hikosaka K, Nakagawa T. NAD Metabolism in Cancer Therapeutics. *Front Oncol* 8: 622, 2018.

104. Yang H, Yang T, Baur JA, Perez E, Matsui T, Carmona JJ, Lamming DW, Souza-Pinto NC, Bohr VA, Rosenzweig A, de Cabo R, Sauve AA, Sinclair DA. Nutrient-sensitive mitochondrial NAD+ levels dictate cell survival. *Cell* 130: 1095-107, 2007.

105. Yang Y, Sauve AA. NAD(+) metabolism: Bioenergetics, signaling and manipulation for therapy. *Biochim Biophys Acta* 1864: 1787-1800, 2016.

106. Ying W. NAD+/NADH and NADP+/NADPH in cellular functions and cell death: regulation and biological consequences. *Antioxid Redox Signal* 10: 179-206, 2008.

107. Yoshino J, Imai S. Accurate measurement of nicotinamide adenine dinucleotide (NAD(+)) with high-performance liquid chromatography. *Methods Mol Biol* 1077: 203-15, 2013.

108. Zaccagnino A, Manago A, Leanza L, Gontarewitz A, Linder B, Azzolini M, Biasutto L, Zoratti M, Peruzzo R, Legler K, Trauzold A, Kalthoff H, Szabo I. Tumor-reducing effect of the clinically

used drug clofazimine in a SCID mouse model of pancreatic ductal adenocarcinoma. *Oncotarget* 8: 38276-38293, 2017.

109. Zamporlini F, Ruggieri S, Mazzola F, Amici A, Orsomando G, Raffaelli N. Novel assay for simultaneous measurement of pyridine mononucleotides synthesizing activities allows dissection of the NAD(+) biosynthetic machinery in mammalian cells. *FEBS J* 281: 5104-19, 2014.

110. Zhang M, Ying W. NAD(+) Deficiency Is a Common Central Pathological Factor of a Number of Diseases and Aging: Mechanisms and Therapeutic Implications. *Antioxid Redox Signal* 30: 890-905, 2019.

111. Zhao FL, Zhang C, Zhang C, Tang Y, Ye BC. A genetically encoded biosensor for in vitro and in vivo detection of NADP(.). *Biosens Bioelectron* 77: 901-6, 2016.

112. Zhao H, Tang W, Chen X, Wang S, Wang X, Xu H, Li L. The NAMPT/E2F2/SIRT1 axis promotes proliferation and inhibits p53-dependent apoptosis in human melanoma cells. *Biochem Biophys Res Commun* 493: 77-84, 2017.

113. Zhao Y, Hu Q, Cheng F, Su N, Wang A, Zou Y, Hu H, Chen X, Zhou HM, Huang X, Yang K, Zhu Q, Wang X, Yi J, Zhu L, Qian X, Chen L, Tang Y, Loscalzo J, Yang Y. SoNar, a Highly Responsive NAD+/NADH Sensor, Allows High-Throughput Metabolic Screening of Anti-tumor Agents. *Cell Metab* 21: 777-89, 2015.

114. Zhao Y, Jin J, Hu Q, Zhou HM, Yi J, Yu Z, Xu L, Wang X, Yang Y, Loscalzo J. Genetically encoded fluorescent sensors for intracellular NADH detection. *Cell Metab* 14: 555-66, 2011.

115. Zhao Y, Zhang Z, Zou Y, Yang Y. Visualization of Nicotine Adenine Dinucleotide Redox Homeostasis with Genetically Encoded Fluorescent Sensors. *Antioxid Redox Signal* 28: 213-229, 2018.

List of publications

(chronological order, 2015-to date, during PhD)

1. Gaudino F., Manfredonia I. et al Subcellular characterization of NAD+ biosynthesis in metastatic melanoma by using organelle-specific biosensors; Antioxid Redox Signal. 2019 Aug 28. doi: 10.1089/ars.2019.7799 (PDF attached).

2. Managò A, Audrito V, Mazzola F, Sorci L, Gaudino F, et al A circulating NAD biosynthetic enzyme is a novel modulator of inflammation; Nature communication, September 2019; doi.org/10.1038/s41467-019-12055-2.

3. Audrito V, Managò A, Gaudino F, Deaglio S. Targeting metabolic reprogramming in metastatic melanoma: The key role of nicotinamide phosphoribosyltransferase (NAMPT); Semin Cell Dev Biol. 2019 May 13. pii: S1084-9521(18)30203-9. doi: 10.1016/j.semcdb.2019.05.001.Review.

4. Audrito V, Managò A, Gaudino F, et al NAD-biosynthetic and consuming enzymes as central players of metabolic regulation of innate and adaptive immune responses in cancer; Frontiers in Immunology, section Cancer Immunity and Immunotherapy, July 2019; doi: 10.3389/fimmu.2019.01720.

5. Ambra A Grolla, Riccardo Miggiano, Daniele di Marino, Michele Bianchi, Alessandro Gori, Giuseppe Orsomando, Federica Gaudino, et al.; NAMPT translocates to the nucleus following interaction with GAPDH to sustain NAD synthesis; Journal of Biological Chemistry (under revision).

6. Audrito V., Managò A., Zamporlini F., Rulli E., Gaudino F. et al Extracellular nicotinamide phosphoribosyltransferase (eNAMPT) is a novel marker for patients with BRAF-mutated metastatic melanoma. Oncotarget. 2018 Apr 10;9(27):18997-19005. doi: 10.18632/oncotarget.24871.

7. Vaisitti T, Gaudino F., et al Targeting metabolism and survival in chronic lymphocytic leukemia and Richter syndrome cells by a novel NF-κB inhibitor. Haematologica. 2017 Nov;102(11):1878- 1889. doi: 10.3324/haematol.2017.173419.

8. Audrito V, Serra S, Stingi A, Orso F, Gaudino F., et al PD-L1 up-regulation in melanoma increases disease aggressiveness and is mediated through miR-17-5p. Oncotarget. 2017 Feb 28;8(9):15894- 15911. doi: 10.18632/oncotarget.15213.

1. Title: Subcellular characterization of NAD^+ biosynthesis in metastatic melanoma by using organelle-specific biosensors

Authors: Federica Gaudino, Ilaria Manfredonia, Antonella Managò, Valentina Audrito, Nadia Raffaelli, Tiziana Vaisitti, Silvia Deaglio.

Original research communication published in Antioxidant and Redox Signaling , August 2019
doi: 10.1089/ars.2019.7799

Individual Contribution:

This work was build and developed as the main research project of my PhD course. Supported by the experience of the Professor Silvia Deaglio, I designed and performed all the experiments shown in the manuscript. In detail, I conducted *in vitro* experiments for the purpose to characterize NAD^+ biosynthesis in metastatic melanoma. To the aim, I used a biochemical approach in which organelles fractionation was followed by western blot analysis of compartment specific NBEs expression. Confocal microscopy was used to support biochemical analysis. From a functional point of view, I generated A375 melanoma cells stably expressing a recently devised NAD^+ biosensor targetable to cytosol, mitochondrion or nucleus. These cell lines were used to quantify subcellular-specific NAD^+ variations as response to the treatments with FK866 (the main NAD^+ biosynthesis inhibitor) or with the precursors of all NAD^+ biosynthetic routes. This required the application of molecular and cellular biology techniques and cytofluorimetric analyses. Together with Silvia Deaglio I interpreted data and wrote the manuscript.

Publications beyond this PhD Thesis (chronological order).

Title: Extracellular nicotinate phosphoribosyltransferase binds Toll like receptor 4 and mediates inflammation

Authors: Antonella Managò, Valentina Audrito, Francesca Mazzola, Leonardo Sorci, Federica Gaudino, Katiuscia Gizzi, Nicoletta Vitale, Danny Incarnato, Gabriele Minazzato, Alice Ianniello, Antonio Varriale, Sabato D'Auria, Giulio Mengozzi, Gianfranco Politano, Salvatore Oliviero, Nadia Raffaelli, Silvia Deaglio.

Research article published in Nature Communication, September 2019 doi.org/10.1038/s41467-019-12055-2

Individual Contribution:

I contributed with experimental support in macrophage differentiation from healthy donor derived peripheral blood mononuclear cells, biochemical and molecular biology assays.

Title: Targeting metabolic reprogramming in metastatic melanoma: The key role of nicotinamide phosphoribosyltransferase (NAMPT)

Authors: Valentina Audrito, Antonella Managò, Federica Gaudino, Silvia Deaglio.

Review article published in Seminars in cells & Developmental Biology, May 2019 doi: 10.1016/j.semcdb.2019.05.001

Individual Contribution:

Together with the co-authors I performed literature search, focusing my attention on the most recent information on NAD^+ biosynthesis compartmentalization and the role of NAD^+ in cancer. I also participated in the revision process of the entire review.

Title: NAD-biosynthetic and consuming enzymes as central players of metabolic regulation of innate and adaptive immune responses in cancer; Frontiers in Immunology, section Cancer Immunity and Immunotherapy

Authors Valentina Audrito, Antonella Managò, Federica Gaudino, Leonardo Sorci, Vincenzo Gianluca Messana, Nadia Raffaelli and Silvia Deaglio.

Review article published in Frontiers in Immunology, July 2019 doi: 10.3389/fimmu.2019.01720

Individual Contribution:

In this review, I contributed to the writing of the role of NAD^+/CD38 metabolic dynamics in T-cells activation.

Title: NAMPT translocates to the nucleus following interaction with GAPDH to sustain NAD synthesis

Authors: Ambra A Grolla, Riccardo Miggiano, Daniele di Marino, Michele Bianchi, Alessandro Gori, Giuseppe Orsomando, Federica Gaudino, Ubaldina Galli, Erika Del Grosso, Francesca Mazzola, Carlo Angeletti, Martina Guarneri, Simone Torretta, Marta Calabrò, Xiaorui Fan, Giorgia Colombo, Cristina Travelli, Francesca Rocchio, James A Wohlschlegel, Silvia Deaglio, Menico Rizzi, Armando A. Genazzani, and Silvia Garavaglia.

Original Research article under review in Journal of Biological Chemistry (under revision)

Individual Contribution:

In this work I performed NAD^+ quantification in nuclei of A375 cells expressing the nuclear NAD^+ biosensor after exposure to UV radiations or H_2O_2 treatments.

Title: Extracellular nicotinamide phosphoribosyltransferase (eNAMPT) is a novel marker for patients with BRAF-mutated metastatic melanoma.

Authors: Valentina Audrito, Antonella Managò, Federica Zmporlini, Elena Rulli, Federica Gaudino, Gabriele Madonna, Stefando D'Atri, Gian Carlo Antonini Cappellini, Paolo Antonio Ascierto, Daniela Massi, Nadia Raffaelli, Mario Mandalà and Silvia Deaglio.

Original research article published in Oncotarget, April 2018, doi:10.18632/oncotarget.24871

Individual Contribution:

In this project I performed biochemical experiments and I have participated to the revision of the manuscript.

Title: Targeting metabolism and survival in chronic lymphocytic leukemia and Richter syndrome cells by a novel NF-κB inhibitor.

Original research article published in Haematologica. 2017 Nov; doi:10.3324/haematol.2017.173419.

Authors: Tiziana Vaisitti, Federica Gaudino, Samedy Ouk, Maria Moscvin, Nicoletta Vitale, Sara Serra, Francesca Arruga, Johannes L. Zakrewski, Hsiou-Chi Liou, John N. Allan, Richard R. Furman and Silvia Deaglio.

Individual Contribution:

In this project I performed biochemical experiments and real time qPCR. I also carried out cytofluorimetric and confocal microcopy experiments and immunohistochemistry and I have participated to the revision of the manuscript as well.

Title: PD-L1 up-regulation in melanoma increases disease aggressiveness and is mediated through miR-17-5p.

Original research article published in Oncotarget. 2017 Feb 28; doi: 10.18632/oncotarget.15213.

Authors: Valentina Audrito, Sara Serra, Aureliano Stingi, Francesca Orso, Federica Gaudino, Cinzia Bologna, Francesco Neri, Giulia Garaffo, Romina Nassini, Gianna Baroni, Eliana Rulli, Daniela Massi, Salvatore Oliviero, Roberto Piva, Daniela Taverna, Mario Mandalà, Silvia Deaglio.

Individual Contribution:

In this project I performed real time qPCR for the quantification of miRNA expression. I also carried out invasion and wound healing assays, viability and immunofluorescence analysis and data processing.